Plant Hydraulic Transport Controls Transpiration ~~Response~~ Sensitivity to Soil Water Stress

Brandon P. Sloan[1,2], Sally E. Thompson[3], and Xue Feng[1,2]

[1]Department of Civil Environmental and Geo-Engineering, University of Minnesota - Twin Cities, Minneapolis, MN 55455
[2]Saint Anthony Falls Laboratory, University of Minnesota - Twin Cities, Minneapolis, MN 55455
[3]Department of Civil, Environmental and Mining Engineering, University of Western Australia, Perth, Australia

Correspondence: Brandon Sloan (sloan091@umn.edu), Xue Feng (feng@umn.edu)

Abstract. Plant transpiration downregulation in the presence of soil water stress is a critical mechanism for predicting global water, carbon, and energy cycles. Currently, many terrestrial biosphere models (TBMs) represent this mechanism with an empirical correction function (β) of soil moisture—a convenient approach that can produce large prediction uncertainties. To reduce this uncertainty, TBMs have increasingly incorporated physically-based Plant Hydraulic Models (PHMs). However, PHMs introduce additional parameter uncertainty and computational demands. Therefore, understanding why and when PHM and β predictions diverge would usefully inform model selection within TBMs. Here, we use a minimalist PHM to demonstrate that coupling the effects of soil water stress and atmospheric moisture demand leads to a spectrum of transpiration response controlled by soil-plant hydraulic transport (conductance). Within this transport-limitation spectrum, β emerges as an end-member scenario of PHMs with infinite conductance, completely decoupling the effects of soil water stress and atmospheric moisture demand on transpiration. As a result, PHM and β transpiration predictions diverge most ~~when conductance is low~~ for soil-plant systems with low hydraulic conductance (transport-limited) ~~,~~ that experience high variation in atmospheric moisture demand ~~variation is high, and soil moisture is moderately available~~ and have moderate soil moisture supply to plants. We ~~apply~~ test these minimalist model results ~~to~~ by land surface modeling ~~of~~ an Ameriflux site. At this transport-limited site, a PHM downregulation scheme outperforms the β scheme due to its sensitivity to variations in atmospheric moisture demand. Based on this observation, we develop a new 'dynamic β' that varies with atmospheric moisture demand—an approach that ~~balances realism with parsimony and~~ overcomes existing biases within β schemes and has potential to simplify existing PHM parameterization and implementation.

1 Introduction

Plants control their ~~water use (i.e.,~~ transpiration (T) ~~)~~ and CO_2 assimilation by adjusting leaf stomatal apertures in response to environmental variations (Katul et al., 2012; Fatichi et al., 2016). In doing so, they mediate the global water, carbon, and energy cycles. The performance of most terrestrial biosphere models (TBMs) relies on accurately representing leaf stomatal responses in terms of stomatal conductance (g_s). Extensive research has established the relationships between g_s and atmospheric conditions like photosynthetically active radiation, humidity, CO_2 concentration, and air/leaf temperature ~~(see Buckley and Mott (2013) and references therein)~~ under well-watered conditions, though the specific forms of these re-

lationships vary ~~(Damour et al., 2010)~~(Damour et al., 2010; Buckley et al., 2014; Buckley, 2017). However, representing the dynamics of g_s in response to soil water stress remains problematic.

Many TBMs represent declining g_s and, in turn, transpiration reduction (i.e., downregulation) in response to soil water stress with an empirical function of soil water availability. This method, known as β (Powell et al., 2013; Verhoef and Egea, 2014; Trugman et al., 2018; Paschalis et al., 2020), reduces ~~transpiration~~ g_s from its peak value under well-watered conditions ($\sout{T_{ww}} g_{s,ww}$), i.e., $\sout{T = \beta \cdot T_{ww} g_s = \beta \cdot g_{s,ww}}$, $0 \leq \beta \leq 1$. (We use the term 'β' in this paper to refer to the downregulation model itself, and the terms 'β function' or 'β factor' to refer to the empirical function and its values, respectively.) The term 'well-watered' refers to moist soil conditions where stomatal aperture is unaffected by soil water uptake, i.e., no soil water stress. Using a β ~~originated~~ function to reduce well-watered transpiration (or g_s) originated, to the best of our knowledge, as a heuristic assumption ~~when modeling flow around roots in soils (Feddes et al., 1978)and~~ in the crop transpiration model, SWATR (Feddes et al., 1978). Since then, it has gained widespread use within TBMs and hydrological models due to its parsimonious form.

However, mounting evidence indicates that using β in TBMs is a major source of uncertainty and bias in plant-mediated carbon and water flux predictions. Multiple studies have implicated the lack of a universal β formulation as a primary source of ~~intermodel~~ inter-model variability in carbon cycle predictions (Medlyn et al., 2016; Rogers et al., 2017; Trugman et al., 2018; Paschalis et al., 2020). For example, different β formulations among nine TBMs ~~were responsible~~ accounted for 40%-80% of ~~intermodel~~ inter-model variability in global gross primary productivity (GPP) predictions (on the order of 3-283% of current GPP) (Trugman et al., 2018). Aside from the uncertainty in functional form, β appears to fundamentally misrepresent the coupled effects of soil water stress and atmospheric moisture demand on stomatal closure. Recent work using model-data fusion at FLUXNET sites highlighted that β ~~is~~ produces stomatal responses that are overly sensitive to soil water stress and unrealistically insensitive to atmospheric moisture demand (Liu et al., 2020). Furthermore, TBM validation experiments have found β schemes produce unrealistic GPP prediction during drought at Amazon rainforest sites (Powell et al., 2013; Restrepo-Coupe et al., 2017) and systematic overprediction of evaporative drought duration, magnitude and intensity (Ukkola et al., 2017) at several Ameriflux sites. The apparent inadequacy of β has lead to the adoption of physically-based Plant Hydraulic Models (PHMs) in TBMs (Williams et al., 2001; Bonan et al., 2014; Xu et al., 2016; Kennedy et al., 2019; Eller et al., 2020; Sabot et al., 2020).

PHMs represent water transport, driven by a gradient of water potential energy, through the soil-plant-atmosphere continuum via flux-gradient relationships (based on Hagen-Poiseuille flow)~~and conductance curves~~, which use measurable soil properties and plant traits as parameters (Mencuccini et al., 2019). The implementation of PHMs in several popular TBMs (e.g., CLM, JULES, etc.) has improved predictions in site-specific GPP and evapotranspiration (ET) predictions (Powell et al., 2013; Bonan et al., 2014; Eller et al., 2020; Sabot et al., 2020; Kennedy et al., 2019) as well as soil water dynamics (Kennedy et al., 2019) compared to β. PHMs also exhibit more realistic sensitivity to atmospheric moisture demand than β (Liu et al., 2020). However, these improvements from PHMs come at the cost of an increased number of plant hydraulic trait parameters and computational burden, which can reduce the ~~robustness and~~ reliability of the predictions (Prentice et al., 2015). Additionally, ~~plant hydraulic traits are difficult to constrain: they~~ obtaining representative plant hydraulic trait values for a soil-plant system is difficult for

two main reasons: i) traits vary widely across and within species (Anderegg, 2015) and exhibit plasticity through ~~adaptation. Furthermore, the traits are measured at~~ acclimation and adaptation (Franks et al., 2014), and ii) trait measurements are typically made at a single point (e.g., stem, branch~~or leaflevels, and scaling them to represent stand or ecosystem behavior remains challenging (Feng, 2020)~~, leaf), which may not be able to reliably scaled to represent whole-plant or ecosystem-level responses due to the effects of nonlinear trait variations along the soil-plant system (Couvreur et al., 2018). These difficulties result in uncertainty in the model predictions that may be further compounded at the ecosystem level (Fisher et al., 2018; Feng, 2020). Consequently, modelers continue to rely on β as a parsimonious alternative to PHMs (Paschalis et al., 2020).

The relative strengths and weaknesses of β and PHMs suggest that informed model selection requires a better understanding of when the complexity of a PHM is justified over the simplicity of β. This paper informs such understanding by: i) analyzing the fundamental differences between PHMs and β~~and their controlling parameters~~, ii) defining the parameters controlling the differences (Sect. ~~3.1-3.2) , ii) demonstrating the environmental conditions where~~ 3.2) and iii) demonstrating how PHMs outperform β for a real soil-plant system (Sect. ~~3.2-3.3), and iii)~~ 3.3). Then, leveraging our theoretical insights~~to~~, we create a new 'dynamic β' ~~that captures the realism of PHMs while retaining the simplicity of the~~ as a potential tool to correct the biases from the original β while reducing the parameter and computational demands of PHMs (Sect. 3.3). To ~~do this~~accomplish these goals, we first analyze a minimalist PHM using a water supply-demand framework, then corroborate the results ~~using~~ for a more widely-used, complex PHM, and~~finally~~, finally, perform a case study with a calibrated land surface model (LSM)~~using~~, which employs β, PHM, and 'dynamic β' downregulation schemes.

2 Methods

2.1 Minimalist PHM

Our minimalist ~~PHM analysis~~ (Sect. 3.1-3.2) ~~uses~~ and complex PHM formulations (Sect. 3.3), illustrated in Fig. 1, rely on a supply-demand framework that conceptualizes transpiration as the joint outcome of soil water supply and atmospheric moisture demand (Gardner, 1960; Cowan, 1965; Sperry and Love, 2015; Kennedy et al., 2019). In this framework, 'supply' refers to the rate of water transport to the leaf mesophyll cells from the soil, into the roots, and through the xylem. 'Demand' refers to the rate of water vapor outflux through the stomata, ~~regulated by~~ driven by the transport capacity of the air surrounding the plant and regulated by the stomatal response to atmospheric conditions ~~(Buckley and Mott, 2013)~~ (Buckley, 2017) and leaf water ~~potential (Jarvis, 1976; Sperry et al., 1998; Klein, 2014; McAdam and Brodribb, 2016; Anderegg et al., 2017) and driven by the transport capacity of the air surrounding the plant~~ status (Klein, 2014; Buckley, 2019). We assume steady-state transpiration fluxes (i.e., supply equals demand), which means we neglect the effects of plant capacitance (Bohrer et al., 2005) and also assume that the mean plant and atmospheric states equilibrate quickly over short timescales.

The minimalist PHM supply (~~T_s^{phm}~~ T_s [$\mathrm{mm\,day^{-1}}$]; Eq. 1 and blue segment in Fig. 1a) is represented by ~~an~~ a steady-state, integrated 1-D flux-gradient relationship, bounded by ~~soil and leaf water potentials~~ the root zone average soil water potential (ψ_s ~~and~~ [MPa]) and leaf water potential (ψ_l [MPa]) and mediated by the bulk conductance along the flowpath ($g_{sp}(\psi)$ ~~).~~ ~~Following Manzoni et al. (2014)~~[$\mathrm{mm\,day^{-1}\,MPa^{-1}}$]). For simplicity, we assume constant soil-plant conductance (g_{sp}) and

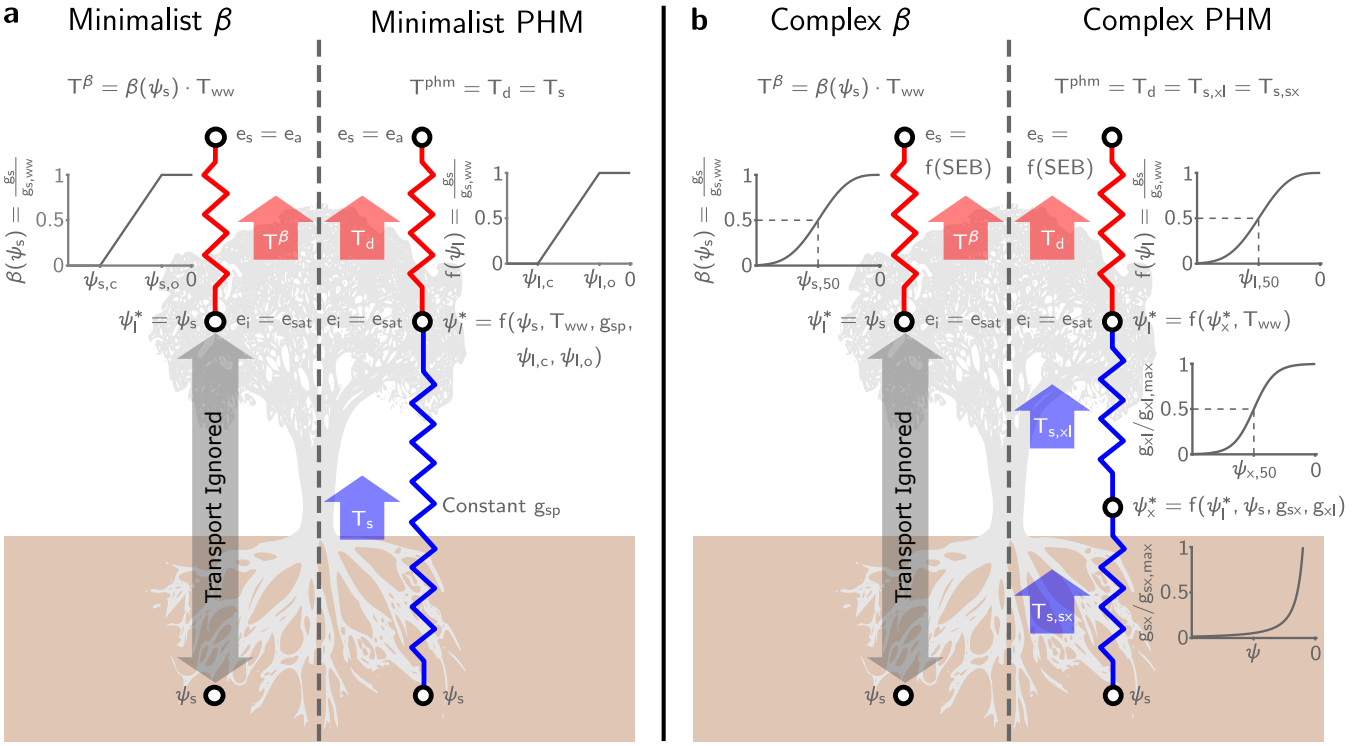

Figure 1. Schematic for the minimalist and complex β and PHM models used in this analysis. The resistors represent the conductance between soil-plant segments (i.e., an analogy to Ohm's Law) that mediate liquid water supply (blue) and atmospheric water vapor demand (red). Next to each resistor the segment-specific conductance downregulation curve dependent on water potential (ψ). The white circles indicate segment endpoints where we calculate the potentials (ψ) for liquid water transport and vapor pressures (e) for water vapor transport. The segment subscripts represent soil (s), xylem (x), leaf (l), inside the leaf (i) and ambient air (a). For water vapor transport, we assume saturation vapor pressure inside the leaf ($e_i = e_{sat}$). Furthermore, we assume the leaf surface vapor pressure (e_s) is the atmospheric vapor pressure (e_a) for the minimalist model, while e_s is a function of the surface energy balance ($f(SEB)$) calculations at each time step for the complex formulation. is a function of the surface energy budget solution at each time step. The thick arrows represent the water transport through each segment calculated by the integrated, steady-state flux-gradient relationships discussed in Sect. 2.1-2.2 and Sect. 2.5. We use the minimalist models (left panel) for Sect. 3.1-3.2 and the complex models (right panel) for the LSM analysis in Sect. 3.3 (Note: We only illustrate a single-leaf formulation here, but see Sect. S2 for full details of the two-leaf implementation.).

~~steady state transpiration to simplify~~ ignore its dependence on water potential (i.e., hydraulic limits (Sperry et al., 1998)).

This assumption simplifies the integral in Eq. 1 to the product of ~~soil-plant conductance and~~ g_{sp} and the water potential difference~~from soil to leaf.~~ , $\psi_s - \psi_l$, which drives the flow.

$$T_s = -\int_{\psi_s}^{\psi_l} g_{sp}(\psi)\, d\psi = g_{sp} \cdot (\psi_s - \psi_l) \tag{1}$$

The minimalist PHM demand (~~T_d^{phm}~~ T_d [mm day^{-1}]; Eq. 2 ~~) consists of a downregulation function ($f(\psi_l)$)multiplied by the~~ and red segment in Fig. 1a) uses a similar conductance-difference formulation (i.e. integrated flux-gradient relationship). Transpiration is driven by the leaf-to-air water vapor pressure deficit (D [mol H_2O/mol air]) and mediated by the well-watered transpiration rate ~~(T_{ww}).~~ stomatal conductance ($g_{s,ww}$ [mol air m^{-2} s^{-1}]), a stomatal closure term ($f(\psi_l)$~~represents stomatal closure under low ψ_l (Jarvis, 1976; Klein, 2014) and can take a piecewise linear form (Eq.3) parametrized by~~), and the leaf area index (LAI [m^2 leaf m^{-2} ground]). Additionally, we convert T_d from a molar flux to a volume flux using the conversion factor C_a (i.e., molar weight of water (M_w [kg mol^{-1}]) divided by water density (ρ_w [kg m^{-3}]) and multiplied by the conversion from m s^{-1} to mm day^{-1}). The driving force D assumes saturation vapor pressure inside the leaf (i.e., $e_i = e_{sat}$) and that the leaf surface (e_s) and atmospheric vapor pressure (e_a) are the same. The parameter $g_{s,ww}$ encapsulates the stomatal response to atmospheric conditions only (i.e., light, temperature, humidity, and CO_2 concentration). We define the ~~leaf water potential at incipient ($\psi_{l,o}$) and complete stomatal closure ($\psi_{l,c}$). T_{ww} is the~~ product of ~~well-watered stomatal conductance (LAI, $g_{s,ww}$) and the vapor pressure deficit (~~and D ~~). For clarity,~~ as the well-watered transpiration rate (T_{ww})—which represents atmospheric moisture demand throughout this paper— and specify its value for the minimalist analysis. The term 'well-watered' refers to abundant soil water conditions under which water transport to the leaves maintains ψ_l high enough to avoid stomatal closure~~; therefore, T_{ww} and~~ . During water-stressed conditions, the $f(\psi_l)$ term represents stomatal closure (i.e., downregulating $g_{s,ww}$~~only depend on atmospheric conditions. In the minimalist analysis, T_{ww} values were selected and not calculated.~~) to lowering leaf water status (Buckley, 2019). We assume a normalized, piecewise linear $f(\psi_l)$ (Eq. 3 and illustrated in Fig. 1a), parametrized by the leaf water potential at incipient ($\psi_{l,o}$) and complete stomatal closure ($\psi_{l,c}$). This simple multiplicative reduction of $g_{s,ww}$ (similar to the approach of Jarvis (1976)) captures the observed non-unique relationship between g_s and ψ_l (Anderegg and Venturas, 2020) while facilitating comparison with the similar minimalist β formulation (see Sect. 2.5).

$$T_s^{phm} = -\int_{\psi_s}^{\psi_l} \frac{K_p(\psi)\, d\psi}{z_{\psi_l} - z_{\psi_s}} = -\int_{\psi_s}^{\psi_l} g_{sp}(\psi)\, d\psi = g_{sp} \cdot \psi_s - \psi_l T_d^{phm} = LAI \cdot f(\psi_l) \cdot g_{s,ww} \cdot D \cdot C_a = f(\psi_l) \cdot T_{ww} \cdot C_a \tag{2}$$

$$f(\psi_l) = \begin{cases} 1 & \psi_l \geq \psi_{l,o} \\ \frac{\psi_{l,c} - \psi_l}{\psi_{l,c} - \psi_{l,o}} & \psi_{l,c} < \psi_l < \psi_{l,o} \\ 0 & \psi_l \leq \psi_{l,c} \end{cases}$$

$$f\left(\psi_l\right) = \frac{g_s(\psi_l)}{g_{s,ww}} = \begin{cases} 1 & \psi_l \geq \psi_{l,o} \\ \frac{\psi_{l,c}-\psi_l}{\psi_{l,c}-\psi_{l,o}} & \psi_{l,c} < \psi_l < \psi_{l,o} \\ 0 & \psi_l \leq \psi_{l,c} \end{cases} \quad (3)$$

~~The steady state transpiration rate for the minimalist PHM (T^{phm}; Eq. 5) is found at the~~

The PHM supply and demand are coupled through their mutual dependence on leaf water potential~~where supply equals demand (ψ_l^*). The equation for ψ_l^* is derived by equating~~. The ψ_l value that balances supply (Eq. 1~~-2 and solving for ψ_l~~) and demand (Eq. 2)~~—~~which we will call ψ_l^* (Eq. 4)~~. Equation 4 is substituted into Eq. 1 to yield T^{phm} (~~—~~yields the steady state transpiration rate for the minimalist PHM (T^{phm}; Eq. 5). The full derivation of ψ_l^* and T^{phm} is shown in ~~section~~ Sect. S1~~of the Supplement~~.

$$T^{phm}\psi_l^* = \frac{\psi_s \cdot (\psi_o - \psi_c) + \frac{T_{ww} \cdot \psi_c}{g_{sp}}}{(\psi_o - \psi_c) + \frac{T_{ww}}{g_{sp}}} \quad (4)$$

$$\psi_l^* T^{phm} = \frac{\psi_s \cdot (\psi_o - \psi_c) + \frac{T_{ww} \cdot \psi_c}{g_{sp}}}{(\psi_o - \psi_c) + \frac{T_{ww}}{g_{sp}}} \begin{cases} T_{ww} & \psi_s > \psi_{l,o} + \frac{T_{ww}}{g_{sp}} \\ T_{ww} \cdot \frac{(\psi_{l,c}-\psi_s)}{(\psi_{l,c}-\psi_{l,o})-\frac{T_{ww}}{g_{sp}}} & \psi_{l,c} < \psi_s \leq \psi_{l,o} + \frac{T_{ww}}{g_{sp}} \\ 0 & \psi_s \leq \psi_{l,c} \end{cases} \quad (5)$$

2.2 Complex PHM

The LSM analysis ~~in this paper~~ (Sect. 3.3) uses a more complex PHM formulation following Feng et al. (2018). The PHM ~~segments~~ separates supply into soil-to-xylem and xylem-to-leaf ~~compartments~~ segments and demand into a leaf-to-atmosphere ~~compartment. The conductance in each compartment consists of a maximum conductance downregulated by a function of water potential . In the supply compartments, the dependence of conductance~~ segment (Fig. 1b). Here, we briefly discuss the complex PHM components for a single big-leaf formulation; however, we refer the reader to Sect. S2-S3 for full model details and parameter values for the two big-leaf formulation used in our LSM.

For PHM supply (T_s; blue segments in Fig. 1b), the water potential gradient drives flow through the soil-plant system mediated by the segment-specific conductance. Unlike the minimalist PHM (Sect. 2.1), we assume the conductance in each segment depends on water potential, which represents 'hydraulic limits' (Sperry et al., 1998) that arise via (i) the inability of roots to remove water from soil pores at low ψ_s and (ii) xylem embolism caused by large hydraulic gradients required under low ψ_s and/or high T_{ww}. The soil-to-xylem conductance (g_{sx} ~~)~~[$\mathrm{mm\,day^{-1}\,MPa^{-1}}$]; Eq. 6 and illustrated in Fig. 1b) is its maximum value ($g_{sx,max}$) downregulated by the unsaturated soil hydraulic conductivity curve (Clapp and Hornberger, 1978), which is parametrized by the saturated soil water potential (ψ_{sat}), soil water retention exponent (b), unsaturated hydraulic

conductivity exponent ($c = 2b + 3$), and a correction factor (~~$d = 4$~~d) to account for roots' ability to reach water (Daly et al., 2004). The xylem-to-leaf conductance (g_{xl} [$\mathrm{m\,s^{-1}\,MPa^{-1}}$]; Eq. 7 and illustrated in Fig. 1b) is its maximum value ($g_{xl,max}$) downregulated by a sigmoidal function (Pammenter and Willigen, 1998), which is parametrized by the vulnerability exponent (a) and the xylem water potential (ψ_x) at 50% loss of conductance ($\psi_{x,50}$). ~~The~~ We estimate the maximum conductance values for each segment ($g_{sx,max}$ and $g_{xl,max}$ ~~values are estimated using~~) with trait-based equations following Feng et al. (2018) (see ~~section S6 of~~ Sect. S2.5.3). Given that conductance varies with water potential, we utilize a Kirchhoff transform (Eq. 8) to approximate the water supply from each segment ($T_{s,sx}$ and $T_{s,xl}$ [$\mathrm{mm\,day^{-1}}$]; Eq. 9-10) as the difference in the matric flux potential (Φ [$\mathrm{mm\,day^{-1}}$]) at the segment endpoints. Therefore, given a value of ψ_s (i.e., root zone average potential) and ψ_l, the ψ_x that balances $T_{s,sx}$ and $T_{s,xl}$—called ψ_x^*—yields the ~~Supplement~~steady-state supply rate (T_s).

$$g_{sx}(\psi) = g_{sx,max} \cdot \left(\frac{\psi_{sat}}{\psi}\right)^{\frac{c-d}{b}} \tag{6}$$

$$g_{xl}(\psi) = g_{xl,max} \cdot \left[1 - \frac{1}{e^{a(\psi-\psi_{x,50})}} \frac{1}{1+e^{a(\psi-\psi_{x,50})}}\right] \tag{7}$$

~~The single demand compartment represents leaf-to-atmosphere conductance (~~

$$\Phi(\psi) = \int_{-\infty}^{\psi} g(\psi')\, d\psi' \tag{8}$$

$$T_{s,sx} = \Phi_{sx}(\psi_s) - \Phi_{sx}(\psi_x) \tag{9}$$

$$T_{s,xl} = \Phi_{xl}(\psi_x) - \Phi_{xl}(\psi_l) \tag{10}$$

The complex PHM demand (T_d [$\mathrm{mm\,day^{-1}}$]; Eq.11 and red segment in Fig. 1b) mirrors the minimalist version (Eq. ~~13) as the stomatal conductance (g_s; Eq. 13) downregulated from its well-watered value ($g_{s,ww}$) using a Weibull function which is parmetrized by a shape factor (b_l) describing stomatal sensitivity and~~ 2) with modifications to fit into a dual-source LSM scheme (Sect. 2.3) that explicitly represents the coupled mass, heat and energy transfer between the plant and its microclimate and the atmosphere. The driving force of transpiration is no longer D but rather the difference between leaf internal (e_i [kPa]) and surface (e_s [kPa]) vapor pressure (normalized by atmospheric pressure (P_{atm} [kPa]) to obtain units $\mathrm{mol\,H_2O/mol\,air}$). We still assume e_i is the ~~leaf water potential at 50% loss of conductance ($\psi_{l,50}$) (Klein, 2014). This Weibull form is similar to the piecewise linear form of $f(\psi_l)$ in the minimalist PHM (Eq. 3~~saturation vapor pressure at leaf temperature (e_{sat}), but ~~is more consistent with formulations common in TBMs (Oleson et al., 2018). The~~ e_s depends on the plant microclimate

determined by the LSM energy balance solution at each time step (see Sect. S2.6). This plant microclimate is coupled to the well-watered stomatal conductance ($g_{s,ww}$ ~~value (Eq. 12)is estimated by the Medlyn optimal stomatal conductance model (Medlyn et al., 2011) which is parametrized by the minimum stomatal conductance (g_o) , Medlyn slope parameter (g_1) , vapor pressure deficit (D~~ [mol air m^{-2} s^{-1}]) via the optimality-based stomatal response model of Medlyn et al. (2011) . The Medlyn model (Eq. 12) depends on the leaf vapor pressure difference ($e_i - e_s$ [kPa]), net CO_2 assimilation rate (A_n [mol CO_2 m^{-2} s^{-1}]), ~~partial pressure of~~ and the leaf surface CO_2 ~~at the leaf surface~~ mole fraction (approximated by the ratio of leaf surface CO_2 partial pressure (c_s ~~) , and atmospheric pressure (~~[kPa]) and P_{atm} ~~). We refer the reader to section S6 and S7 of the Supplement for full details and parameter values.~~ to give units [mol CO_2/mol air]) and is parametrized by the minimum stomatal conductance (g_o [mol air m^{-2} s^{-1}]) and a slope parameter (g_1 [$kPa^{0.5}$]). Furthermore, we couple $g_{s,ww}$ to the Farquhar et al. (1980) photosynthesis model through A_n to ensure CO_2 diffusion into the leaf balances carbon assimilation (Collatz et al., 1991) (see Sect. S2.4). As in the minimalist model, the product of $g_{s,ww}$, driving force, and LAI yields the well-watered transpiration rate, T_{ww}, which we take to represent atmospheric moisture demand. Under water-stressed conditions, we keep a Jarvis-like stomatal closure term ($f(\psi_l)$) to downregulate $g_{s,ww}$ because it facilitates easy comparisons between our minimalist and complex formulations. However, we upgrade $f(\psi_l)$ from a piecewise linear form (Eq. 3) to a more realistic Weibull form (Eq. 13 and illustrated in Fig. 1b) parametrized by a shape factor (b_l) describing stomatal sensitivity and the leaf water potential at 50% loss of conductance ($\psi_{l,50}$ [MPa]) (Klein, 2014; Kennedy et al., 2019).

~~$$g_s = g_{s,ww} \cdot e^{-\left(\frac{\psi_l}{\psi_{l,50}}\right)^{b_l}}$$~~

$$T_d = LAI \cdot f(\psi_l) \cdot g_{s,ww} \cdot \frac{e_i - e_s}{P_{atm}} \cdot C_a = f(\psi_l) \cdot T_{ww} \cdot C_a \tag{11}$$

~~$$g_{s,ww} = g_o + \left(1 + \frac{g_1}{\sqrt{D}}\right) \cdot \frac{1.6 \cdot A_n}{c_s / P_{atm}}$$~~

$$g_{s,ww} = g_o + \left(1 + \frac{g_1}{\sqrt{e_i - e_s}}\right) \cdot \frac{1.6 \cdot A_n}{c_s / P_{atm}} \tag{12}$$

~~The steady-state solution of the complex PHM requires finding the leaf (ψ_l^*)and xylem water potential (~~

$$f(\psi_l) = \frac{g_s(\psi_l)}{g_{s,ww}} = 2^{-\left(\frac{\psi_l}{\psi_{l,50}}\right)^{b_l}} \tag{13}$$

As in the minimalist PHM, the complex PHM supply and demand are coupled through their mutual dependence on ψ_l. The ψ_l^* that balances T_s (found at ψ_x^* ~~) that balance transport in the three compartments. To calculate supply in each compartment ($T_{s,sx}$ and $T_{s,xl}$) , we use a Kirchhoff transform to account for conductance varying with water potential along the flow path~~

(for Eq. 8) (Sperry et al., 1998) and take the difference in the matric flux potential (Φ) at the segment endpoints (Eq. 9-10) . The demand (T_d; and T_d (Eq. 11) is the stomatal conductance scaled by leaf area index (LAI)and multiplied by D. The values of yields the steady-state transpiration rate for the complex PHM (T^{phm}). We numerically calculate this solution by recasting Eq. 9-11 as a nonlinear least squares problem and finding the ψ_l^* and ψ_x^* that balance flow in each compartment are found using nonlinear least squares. The single big-leaf formulation outlined here has been extended to a two-big leaf formulation used in the LSM analysis (see section S6 of the Supplement for full details). Equations 9-11 contain constants for the latent heat of vaporization ($\mathcal{L}_v$), density of water (ρ_w), density of air (ρ_a), molar density of an ideal gas (ρ_m), and the ratio of molar weight of water to air (ε) to convert transpiration fluxes to units of ensure mass balance between the segments (see Sect. S2.5.3).

$$\Phi(\psi) = \int_{-\infty}^{\psi} g(\psi')\, d\psi'$$

$$T_{s,sx} = [\Phi_{sx}(\psi_s) - \Phi_{sx}(\psi_x)] \cdot \rho_w \cdot \mathcal{L}_v$$

$$T_{s,xl} = [\Phi_{xl}(\psi_x) - \Phi_{xl}(\psi_l)] \cdot \rho_w \cdot \mathcal{L}_v$$

$$T_d = LAI \cdot g_s \cdot D \cdot \frac{\mathcal{L}_v \cdot \rho_a \cdot \rho_m \cdot \varepsilon}{P_{atm}}$$

2.3 LSM Description and Calibration

The LSM created for this work We created an LSM to allow testing of several transpiration downregulation schemes (Sect. 3.3) and removal of modules (e.g. subsurface heat and mass transfer) that would unnecessarily complicate our comparisons. Our LSM is a dual-source, 2-big leaf two big-leaf approximation (Bonan, 2019) adapted from CLM v5 (Oleson et al., 2018) with several key simplifications: 1i) steady-state conditions , 2)negligible (i.e., no above ground mass, heat or energy storage), ii) neutral atmospheric stability, 3) use of the Goudriaan and van Laar iii) implemented the Goudriaan and Laar (1994) radiative transfer model (Goudriaan and Laar, 1994), and 4) forced in lieu of the two-stream approximation (Oleson et al., 2018), and iv) forced LSM with soil moisture, soil heat flux and radiative forcing data. Our simplified LSM allowed parallel computation and removal of confounding model structural errors. down-welling radiation data. We refer the reader to section S6 of the Supplement Sect. S2 for full model details and justifications. The model was formulated We formulated the LSM in MATLAB and codes will be made available online with acceptance of this manuscripthave made the codes available online.

We ran five separate LSMs for this analysis, each with a created separate LSM versions to test five different transpiration downregulation scheme: 1schemes: i) well-watered (no downregulation), 2ii) a single β (β_s) with static parameters, 3iii) a β

separately applied to sunlit and shaded leaf areas (β_{2L}) with static parameters, ~~4~~iv) a 'dynamic β' with parameters dependent on T_{ww} (β_{dyn}), and ~~5~~v) a PHM. We calibrated the ~~LSM with PHM downregulation scheme by simulating~~ PHM version using a two-step approach. First, we simulated 13,600 parameter sets using Progressive Latin Hypercube Sampling (Razavi et al., 2019) on 15 ~~selected~~ soil and plant parameters ~~. The~~ (Table S6) and selected the best parameter set ~~was selected by~~ based on a comparison of RMSE, correlation coefficient, percent bias and variance ~~with~~ to Ameriflux evapotranspiration, sensible heat flux, gross primary productivity, and net radiation site data ~~. We provide full calibration details in section S5 of the Supplement.~~ (Fig. S5-S8). Unfortunately, the best parameter set contained an unrealistically low $\psi_{l,50}$ value for ponderosa pine compared to observations (DeLucia and Heckathorn, 1989). Therefore, as a second step, we adjusted the $\psi_{l,50}$ and several other soil and plant parameters to more realistic values while ensuring that they replicate the transpiration downregulation behavior of the original parameter set. These parameter adjustments had minimal impact on LSM predictions as the underlying equations are highly nonlinear and multiple parameter sets can give near equivalent results (i.e., equifinality). We refer the reader to Sect. S4 for a more detailed account of calibration.

We ~~fit the three LSMs with~~ parametrized the three LSM versions containing the β schemes by calibrating the respective β functions to the relative transpiration outputs (T/T_{ww}) of the calibrated ~~LSM, while~~ PHM version, while we ran the well-watered ~~LSM was run with~~ version using the calibrated parameters and downregulation turned off. The choice to calibrate a single LSM version ensured that the performance differences between the schemes would be due to the PHM representing plant water use more realistically and not to the artifact of differing parameter fits between ~~models~~LSM versions. We refer the reader to ~~section S2~~Sect. S6.2 ~~of the Supplement~~ for specific details of the parameter fits for the β schemes.

2.4 Site Description and Forcing Data

We ~~selected the~~ calibrated and forced the LSM with half-hourly data from the US-Me2 "Metolius" Ameriflux site (Irvine et al., 2008)~~for our modeling case study due to its comprehensive atmospheric and subsurface data availability~~. The site consists of intermediate-age ponderosa pine trees on sandy loam soil in the Metolius River Basin in Oregon, USA. ~~Previous modeling (Schwarz et al., 2004) and measured soil parameters and hydraulic traits (Irvine et al., 2008) helped guide calibration. Volumetric soil water content and soil temperature measurements over multiple depths and years enabled the model results to be tested against the selection of different soil moisture depths to represent plant water availability.~~ We selected this site specifically for its subsurface soil moisture and temperature profiles as well as its separate measurements of photosynthetically active radiation (PAR) and near infrared radiation (NIR). We used these boundary condition data to force the LSM in lieu of solving one-dimensional mass and heat transfer equations and atmospheric radiation partitioning models. In particular, we forced the LSM with root zone averaged soil water potential (ψ_s; estimated from measured soil water content and a pedotransfer function) and the ground heat flux measurements. We selected the measurement depth of 50 cm to represent ψ_s based on the deviation of measured GPP from its mean in relation to measured soil water content and vapor pressure deficit (Fig. S10). The 50 cm measurements showed clear GPP downregulation under water stress. Furthermore, the depth seemed reasonable given previous modeling at this site estimated an effective rooting depth of 1.1 m (Schwarz et al., 2004). The atmospheric forcing for the LSM consisted of incoming direct and diffuse NIR and PAR fluxes, CO_2 concentration, atmospheric pressure, vapor

pressure, temperature and wind velocity at the measurement tower height of 32 m. Full description of the forcing data is given in ~~section S4 of the Supplement.~~ Sect. S5.

2.5 β Formulations

~~As mentioned previously, the~~ The β ~~transpiration downregulation model does not have a universal formulation.~~ function empirically represents stomatal closure to declining leaf water status caused by soil water stress. By design, β ~~functions have been heuristically defined using a variety of water supply proxies including ψ_l (Jarvis, 1976),~~ makes the simplifying assumption that stomata respond directly to soil water status (to avoid the complexity of implementing a PHM shown in Fig. 1), which is readily available in TBM subsurface hydrology schemes as ψ_s ~~(Verhoef and Egea, 2014), and~~ or volumetric soil water content (θ_s)~~(Verhoef and Egea, 2014). Additionally, once the~~ . This heuristic approach leads to multiple β functions based on modeler preference (see Supplement of Trugman et al. (2018) for list of differing β formulations common to TBMs). Furthermore, even if a universal β function ~~is selected, the choice remains of where~~ existed, there is open debate on how to apply the β factor (Egea et al., 2011); some TBMs apply the β factor directly to ~~T_{ww}, whereas others apply it to parameters that control T_{ww}, like~~ stomatal conductance (Kowalczyk et al., 2006; De Kauwe et al., 2015; Wolf et al., 2016) whereas others indirectly affect stomatal conductance by applying the β factor to photosynthetic parameters (Zhou et al., 2013; Lin et al., 2018; Kennedy et al., 2019). Here, we select a single β formulation that easily compares with the demand component of our PHM. Selecting a different β formulation could alter our values; however, we do not expect our main conclusions about β and PHM differences to change as long as two criteria are met. First, the stomatal downregulation factors for the PHM ($f(\psi_l)$) and β ($\beta(\psi_s)$) are applied consistently in the transpiration downregulation scheme (to either $g_{s,ww}$ ~~(Kowalczyk et al., 2006) or maximum photosynthetic rates (Zhou et al., 2013; Lin et al., 2018; Kennedy et al., 2019). Here, we have elected to define~~ or photosynthetic parameters). Second, if β is in terms of θ_s, a curvilinear form must be used (Egea et al., 2011) to ensure β can be mapped approximately to the water potential space of our analysis.

In this paper, we have defined the β function in terms of ψ_s and apply the β factor directly to $g_{s,ww}$ and, in turn, T_{ww} (Eq. 14) ~~as it mirrors the PHM demand equations~~for three key reasons: i) water transport through the soil-plant-atmosphere continuum follows a gradient of water potential, not water content, ii) β using ψ_s rather than θ_s produces more realistic downregulation behavior compared to data (Verhoef and Egea, 2014), and iii) applying the β factor to $g_{s,ww}$ directly corresponds to the PHM demand in both minimalist and complex formulations. In the minimalist analysis (Sect. 3.1-3.2), $\beta(\psi_s)$ (Eq. 15 and illustrated in Fig. 1a) takes a piecewise linear form (analogous to Eq. 3) which is parametrized by the soil water potential at incipient ($\psi_{s,o}$) and complete stomatal closure ($\psi_{s,c}$). Similarly, in the LSM analysis (Sect. 3.3), $\beta(\psi_s)$ (Eq. 16 and illustrated in Fig. 1b) takes a Weibull form (analogous to Eq. 13) parametrized by the soil water potential at 50% loss of stomatal conductance ($\psi_{s,50}$) and a stomatal sensitivity parameter (b_s). The LSM analysis uses two versions of ~~Equation 16: 1~~Eq. 16: i) a static version with

constant b_s and $\psi_{s,50}$ (used by the β_s and β_{2L} schemes), and ~~2~~ii) a dynamic version where b_s and $\psi_{s,50}$ are linear functions of T_{ww} (used by the β_{dyn} scheme). We refer the reader to Fig. S12 for illustrations of the different β versions.

$$T^{\beta} = \beta(\psi_s) \cdot T_{ww} \tag{14}$$

$$\beta(\psi_s) = \begin{cases} 1 & \psi_s \geq \psi_{s,o} \\ \frac{\psi_{s,c} - \psi_s}{\psi_{s,c} - \psi_{s,o}} & \psi_{s,c} < \psi_s < \psi_{s,o} \\ 0 & \psi_s \leq \psi_{s,c} \end{cases} \tag{15}$$

$$\beta(\psi_s, T_{ww}) = e2^{-\left(\frac{\psi_s}{\psi_{s,50}(T_{ww})}\right)^{b_s(T_{ww})}} \tag{16}$$

3 Results

3.1 β as a Limiting Case of PHMs with Infinite Conductance

~~Looking at~~ The supply-demand framework reveals that the minimalist PHM and β ~~models in a supply-demand framework reveals their fundamental differences~~fundamentally differ in their coupling of the effects of soil water stress (represented by ψ_s) and atmospheric moisture demand (represented by T_{ww}) on transpiration. The PHM supply lines (red lines in Fig. 2a) illustrate ~~water transport from soil-to-leaf~~ soil-to-leaf water transport (Eq. 1) at a fixed soil water availability (ψ_s) ~~with~~ under increasing pull from the leaf (lower ψ_l) and constant soil-plant conductance (g_{sp}; supply line slope). The PHM demand lines (black lines in Fig. 2a) illustrate transpiration ~~rate decline (due to~~ reduction under lower ψ_l (from stomatal closure) ~~with lower ψ_l for two atmospheric moisture demands, represented by the well-watered transpiration rate (~~for two T_{ww} ~~). The intersection of the~~ values. The supply and demand lines ~~in Fig. 2a is~~ intersect at the minimalist PHM solution (ψ_l^* and T^{phm}; Eq. ~~5) at the leaf water potential (ψ_l^*; Eq. 4) that equates supply with demand. The difference between ψ_s and ψ_l^* is the water potential difference ($\Delta\psi$) that drives flow through the soil-plant system mediated by the soil-plant conductance (g_{sp} and slope of supply lines). The~~ 4-5). Therefore, the minimalist PHM couples the effects of soil water stress to atmospheric moisture demand on transpiration downregulation because leaf water potential ~~(ψ_l^*) responds to both~~ responds to ψ_s and T_{ww} until ~~the equilibrium transpiration is reached.The empirical~~ it reaches the point of steady-state transpiration (i.e., $T^{phm}(\psi_l^*) = T_s(\psi_l^*) = T_d(\psi_l^*)$).

The minimalist β ~~does not readily map to our supply-demand framework since~~ transpiration rate (T^{β}, Eq. 14) ignores this coupling as the β function ~~is a lumped representation of the~~ depends only on ψ_s and independently reduces T_{ww} (shown in Fig. 1). The conditions leading to the decoupling in β only arise if the supply lines are vertical (Fig. 2b), which results in the relative transpiration (T^{β}/T_{ww}) depending on ψ_s only (single curve in Fig. 2d). Since g_{sp} is the supply line slope (Eq. 1), β represents a limiting case of the PHM in which the soil-plant system ~~. However, the~~ is infinitely conductive. More specifically,

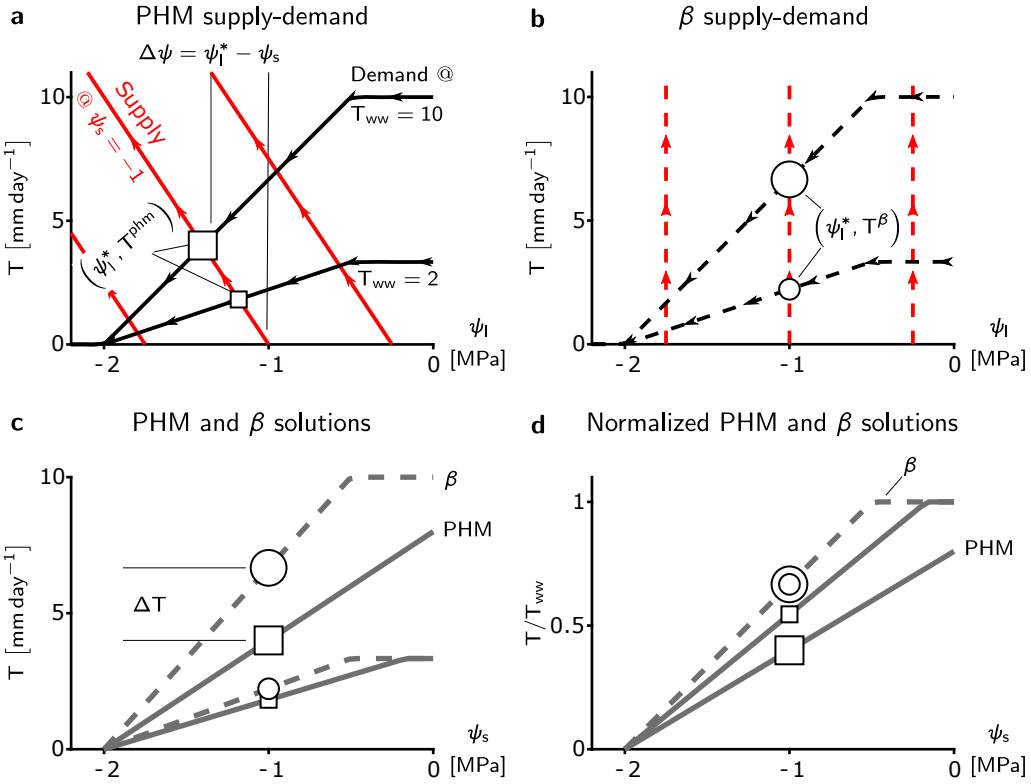

Figure 2. Fundamental differences between minimalist PHM and β. **a-b,** Supply (red) and demand (black) curves for PHM (**a**, solid lines) and β (**b**, dashed lines) under varying leaf water potentials (ψ_l). The squares (circles) represent the PHM (β) solution — i.e., the ψ_l^* where supply equals demand — for a single soil water availability (ψ_s) and two atmospheric moisture demands (T_{ww}). These markers carry through panels **c** and **d** to illustrate how the solutions between the PHM and β diverge at a single ψ_s. The relative size of the markers indicates corresponding T_{ww}. The water potential difference $\Delta\psi$ required to transport water from soil to leaf is shown in panel **a** for $\psi_s = -2$ MPa and $T_{ww} = 10$ mm day^{-1}. **c**, Solutions of panels **a** and **b** mapped to ψ_s, where ΔT is the difference between PHM and β transpiration estimates at $\psi_s = -2$ MPa and $T_{ww} = 10$ mm day^{-1}. **d**, Relative transpiration, in which solutions in panel **c** are normalized by T_{ww}. The β solutions collapse to a single curve, whereas the PHM solutions depend on T_{ww}.

as g_{sp} increases, the leaf water potential approaches the soil water potential ($\psi_l^* \to \psi_s$; Eq. 17) and the PHM transpiration rate approaches the β transpiration rate (~~T^{β}, Eq. 14) decouples the effects of soilwater stress and atmospheric moisture demand on downregulation: the~~ $T^{phm} \to T^{\beta}$; Eq. 18). Therefore, the $\beta(\psi_s)$ function (Eq. 15) equals the $f(\psi_l)$ function (Eq. 3) in PHMs and represents stomatal closure to declining leaf (or soil) water potential. In summary, the empirical β ~~function depends only~~ physically represents an infinitely conductive soil-plant system where stomata close in response to leaf water potential that depends solely on soil water ~~availability, and T_{ww} depends only on atmospheric conditions~~potential with which it is equilibrated.

Fundamental differences between minimalist PHM and β. **a-b,** Supply (red) and demand (black) curves for PHM (**a**, solid lines) and β (**b**, dashed lines) under varying leaf water potentials (ψ_l). The squares (circles) represent the PHM (β) solution — i.e., the ψ_l^* where supply equals demand — for a single soil water availability (ψ_s) and two atmospheric moisture demands (T_{ww}). These markers carry through panels **c** and **d** to illustrate how the solutions between the PHM and β diverge at a single ψ_s. The relative size of the markers indicates corresponding T_{ww}. The water potential difference $\Delta\psi$ required to transport water from soil to leaf is shown in panel **a** for $\psi_s = -2$ MPa and $T_{ww} = 150$ W m^{-2}. **c**, Solutions of panels **a** and **b** mapped to ψ_s, where ΔT is the difference between PHM and β transpiration estimates at $\psi_s = -2$ MPa and $T_{ww} = 150$ W m^{-2}. **d**, Relative transpiration, in which solutions in panel **c** are normalized by T_{ww}. The β solutions collapse to a single curve, whereas the PHM solutions depend on T_{ww}.

$$\lim_{g_{sp}\to\infty}[\psi_l^*] = \lim_{g_{sp}\to\infty}\left(\frac{\psi_s\cdot(\psi_o-\psi_c)+\frac{T_{ww}\cdot\psi_c}{g_{sp}}}{(\psi_o-\psi_c)+\frac{T_{ww}}{g_{sp}}}\right) = \psi_s \tag{17}$$

$$\lim_{g_{sp}\to\infty}(\Delta T) = \lim_{g_{sp}\to\infty}\left(T^{phm}-T^{\beta}\right) = \lim_{g_{sp}\to\infty}\left(T_{ww}\cdot\left[\frac{(\psi_{l,c}-\psi_s)}{(\psi_{l,c}-\psi_{l,o})-\frac{T_{ww}}{g_{sp}}}-\frac{(\psi_{l,c}-\psi_s)}{(\psi_{l,c}-\psi_{l,o})}\right]\right) = 0 \tag{18}$$

The coupling inherent to the PHM PHM coupling results in greater transpiration downregulation compared to β under the same environmental conditions (Fig. 2c). For a given soil water stress (ψ_s), β downregulates transpiration at assumes $\psi_s = \psi_l^*$ and downregulates any atmospheric moisture demand (T_{ww}) value a fixed proportion based on ψ_s only (i.e., it scales linearly with T_{ww}); hence, it can be modeled with a single curve (Fig. 2d). Unlike βConversely, the PHM downregulates transpiration at a greater proportion with increasing atmospheric moisture demand (i.e., it scales nonlinearly with T_{ww}) , and thus must be described as a function of both ψ_s and T_{ww}. Physically, this result stems from a larger (with finite conductance) requires a water potential difference ($\Delta\psi = \psi_s - \psi_l^*$) , and thus a lower ψ_l, required for transport through the soil-plant system under higher atmospheric moisture demand, resulting in to transport water from soil-to-leaf; therefore, ψ_l^* must be less than ψ_s and greater stomatal closure and thus further downregulation (i.e., smaller transpiration relative to T_{ww} in results (Fig. 2d).

The physical conditions leading to the empirical β assumptions result from supply-demand curves that independently account for the effects of soil water stress and atmospheric moisture demand on transpiration downregulation. This situation only arises when the supply lines are vertical (Fig. 2b), resulting in $\psi_l^* = \psi_s$ and the relative transpiration c). Furthermore, the PHM downregulates transpiration at a greater proportion with increasing T_{ww} (i.e., it scales nonlinearly with T_{ww}) as it requires a greater $\Delta\psi$ and lower ψ_l^* (T^{β}/T_{ww}) collapsing to a single curve (Fig. 2d).Since g_{sp} represents the supply line slope (Eq. 1), β is revealed as a limiting case of the PHM in which the soil-plant system is infinitely conductive. We can formally show this limiting behavior in Eq. 17 and 18, where ψ_s approaches ψ_l^* and the difference in PHM and β solutions (ΔT) approaches 0 as $g_{sp} \to \infty$. Interpreted this way, the $\beta(\psi_s)$ function (Eq. 15)represents stomatal closure to declining leaf water potential because of its equivalence to $f(\psi_l)$ (Eq. 3) in PHMs. Therefore, a physical interpretation of β is transpiration downregulation due purely to stomatal closure as leaf water potentials decline, occurring in an infinitely conductive soil-plant system that

~~causes water potential to remain unchanged between soil and leaf~~2d). Hence, PHMs require transpiration downregulation to be described as a function of both ψ_s and T_{ww}.

$$\lim_{g_{sp}\to\infty}[\psi_l^*] = \lim_{g_{sp}\to\infty}\left(\frac{\psi_s\cdot(\psi_o-\psi_c)+\frac{T_{ww}\cdot\psi_c}{g_{sp}}}{(\psi_o-\psi_c)+\frac{T_{ww}}{g_{sp}}}\right) = \psi_s$$

$$\lim_{g_{sp}\to\infty}(\Delta T) = \lim_{g_{sp}\to\infty}\left(T^{phm}-T^{\beta}\right) = \lim_{g_{sp}\to\infty}\left(T_{ww}\cdot\left[\frac{(\psi_{l,c}-\psi_s)}{(\psi_{l,c}-\psi_{l,o})-\frac{T_{ww}}{g_{sp}}}-\frac{(\psi_{l,c}-\psi_s)}{(\psi_{l,c}-\psi_{l,o})}\right]\right) = 0$$

These minimalist model results suggest that the range of soil-plant conductances (g_{sp}) can generate a spectrum of possible transpiration responses to soil water stress (and atmospheric moisture demand). Two classes of behaviors emerge—one in a '~~supply-limited~~soil-limited' soil-plant system, in which g_{sp} is large enough for $\psi_l \approx \psi_s$, thus decoupling the effects of soil water stress and atmospheric moisture demand while allowing the relative transpiration to vary only with ψ_s (Fig. 2d). The other class of behavior arises in 'transport-limited' systems with finite g_{sp}, in which a non-negligible water potential difference ($\Delta\psi$) is required to transport the water to the leaf, resulting in additional downregulation compared to ~~supply-limited~~ soil-limited systems (Fig. 2d) and requiring relative transpiration to depend on both ψ_s and T_{ww}.

3.2 Parameters Controlling the Divergence of β and PHMs

The differences in PHM and β transpiration estimates (ΔT) depends not only on g_{sp}, but also on soil water availability (ψ_s), atmospheric moisture demand (T_{ww}) and plant water use strategy ($\psi_{l,c}-\psi_{l,o}$). To disentangle these joint dependencies, we adjust a single variable and explore the impact on ΔT using the supply and demand lines (Fig. 3). ~~Changes in~~ The translation of supply lines represents ψ_s ~~are represented by the translation of the supply lines (~~changes (indicated in Fig. 3a,c,e) and ~~result in~~ produces a non-monotonic ~~behaviors in~~ relationship with ΔT over the range of soil water stress (i.e., $\psi_{l,c} < \psi_s < \psi_{l,o} + T_{ww}/g_{sp}$) (Fig. 3b,d,f). The peak ΔT occurs at the incipient point of stomatal closure ($\psi_{l,o}$) because i) when $\psi_s < \psi_{l,o}$, transpiration begins to decrease, and in its extreme limit, transpiration (and thus ΔT) approaches 0 and ii) when $\psi_s > \psi_{l,o}$, the effects of downregulation diminish in both models. The ΔT-ψ_s behavior acts as a baseline relationship in the following analysis of g_{sp}, T_{ww}, and $\psi_{l,c}-\psi_{l,o}$ controls.

The ΔT-ψ_s ~~non-monotonic behavior inversely scales with~~ relationship increases with lower g_{sp} ~~, as decreasing the soil-plant conductance (and thus increasing~~ (Fig. 3b; greater transport-limitation) ~~results in~~ because flatter supply lines ~~and greater~~ increase $\Delta\psi$ (Fig. 3a)~~. Furthermore, the range of~~ , requiring greater stomatal closure and hence additional downregulation for a PHM compared to β. Similarly, higher T_{ww} increases ΔT-ψ_s ~~with higher ΔT increases due to increase in the~~ relationship (Fig. 3d), although the increase in $\Delta\psi$ stems from steeper demand line slope (Fig. 3c). In addition to increasing ΔT at each ψ_s value, the effects of g_{sp} and T_{ww} increase the range of soil water stress ~~for the PHM. The ΔT-ψ_s behavior also scales with~~ above $\psi_{l,o}$ (up to saturated soil water potential). This result indicates that PHMs can model transpiration downregulation under moist soil conditions that β potentially misses as it does not account for large $\Delta\psi$ values from transport-limitation and/or high atmospheric moisture demand~~(Fig. 3d) as greater demand line slope results in greater $\Delta\psi$ (~~. Finally, as g_{sp} increases (soil-limited)

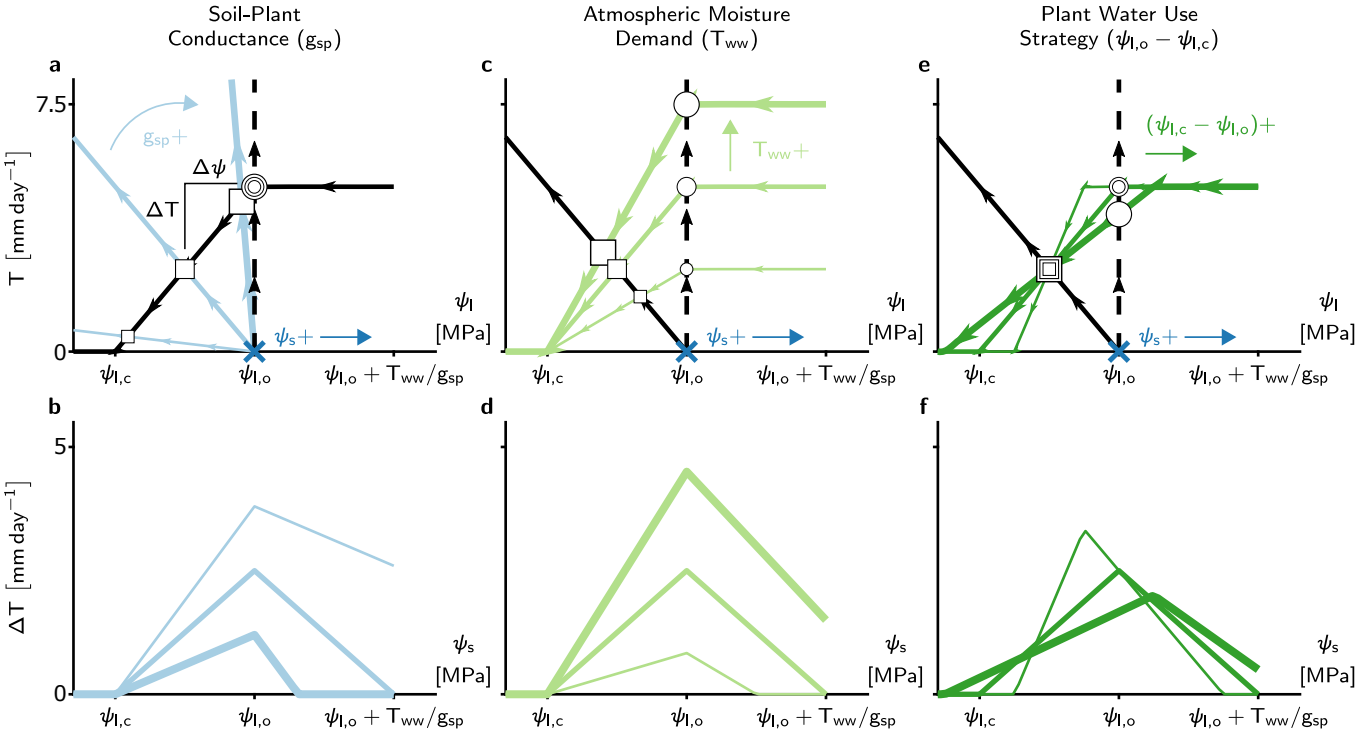

Figure 3. The effect of soil water potential (ψ_s), soil-plant conductance (g_{sp}), atmospheric moisture demand (T_{ww}) and plant water use strategy ($\psi_{l,o} - \psi_{l,c}$) on differences between the minimalist PHM and β models (ΔT). **a,c,e,** Supply-demand curves at a single soil water availability (indicated by the dark blue x at $\psi_s = \psi_{l,o}$), for three prescribed values of g_{sp}, T_{ww}, and $\psi_{l,o} - \psi_{l,c}$, respectively. Each parameter (g_{sp}, T_{ww}, or $\psi_{l,o} - \psi_{l,c}$) is set at 50% above (below) its base values at $g_{sp} = 10\,\mathrm{mm\,day^{-1}\,MPa^{-1}}$, $T_{ww} = 5\,\mathrm{mm\,day^{-1}}$, $\psi_o = -1\,\mathrm{MPa}$, and $\psi_o = -2\,\mathrm{MPa}$ using thick (thin) colored lines. The squares (circles) indicate the PHM (β) solutions, with size corresponding to magnitude of the changing parameter values. Note: the vertical distance between correspondingly sized circle and square is ΔT and horizontal distance is $\Delta\psi$. **b,d,f,** The ΔT results from the panels **a**, **c**, and **e** calculated for a range of ψ_s with line thickness proportional to parameters in the aforementioned panels (e.g., thick blue line in panel **b** corresponds to 50% increase in g_{sp} shown in panel **a**). The x-axes are mapped from ψ_l in the top panels to ψ_s in the bottom panels.

and T_{ww} decreases, ΔT tends to zero, once again, for slightly different reasons: for g_{sp}, the supply lines approach the β assumption (vertical dashed lines in Fig. 3~~c). Lastly, the~~ a), whereas for T_{ww}, transpiration approaches zero.

Lastly, we explore the effect of plant water use strategy ($\psi_{l,c} - \psi_{l,o}$)~~approximates how sensitive stomatal closure is~~ —which approximates the sensitivity of stomatal closure to ψ_l~~. A more aggressive~~ —on ΔT. Altering $\psi_{l,c} - \psi_{l,o}$ does not affect $\Delta\psi$ like the other three variables; however, it modifies the range of soil water stress and redistributes ΔT to conserve the total error over the range. For example, a more aggressive plant water use strategy—closing stomata over a narrower range of ψ_l and ψ_s~~ increases~~ —creates a narrower range of soil water stress with a more peaked ΔT~~as the demand lines becomes more vertical~~ -ψ_s relationship due to more vertical demand lines (Fig. 3e). ~~However, this results in a narrower~~ Therefore, whether

the plant water use strategy could amplify or diminish ΔT for a soil-system relies on how site-specific soil moisture variability overlaps with the range of soil water stress ~~meaning periods of significant ΔT may occur infrequently~~ (Fig. 3f).

In summary, this ~~analysis suggests that~~ minimalist analysis suggest PHMs are most needed to represent transport-limited soil-plant systems under high atmospheric moisture demand ~~variability~~ and moderate soil water ~~stress, especially if downregulation occurs abruptly as a function~~ availability. Plant water use will modulate these results; however, the impact depends on how site-specific soil moisture variability overlaps with the range of soil water stress. ~~The reason PHMs are needed for high atmospheric moisture demand variability is that β is empirical and could be fit to observations at differing T_{ww} values. We discuss this point more thoroughly in the Sect. 3.3.~~

~~The effect of soil water potential (ψ_s), soil-plant conductance (g_{sp}), atmospheric moisture demand (T_{ww}) and plant water use strategy ($\psi_{t,o} - \psi_{t,c}$) on differences between the minimalist PHM and β models (ΔT). **a,c,e,** Supply-demand curves at a single soil water availability (indicated by the dark blue x at $\psi_s = \psi_{t,o}$), for three prescribed values of g_{sp}, T_{ww}, and $\psi_{t,o} - \psi_{t,c}$, respectively. Each parameter (g_{sp}, T_{ww}, or $\psi_{t,o} - \psi_{t,c}$) is set at 50% above (below) its base values at $g_{sp} = 100\,\mathrm{W\,m^{-2}\,MPa^{-1}}$, $T_{ww} = 75\,\mathrm{W\,m^{-2}}$, $\psi_o = -1\,\mathrm{MPa}$, and $\psi_o = -2\,\mathrm{MPa}$ using thick (thin) colored lines. The squares (circles) indicate the PHM (β) solutions, with size corresponding to magnitude of the changing parameter values. Note: the vertical distance between correspondingly sized circle and square is ΔT and horizontal distance is $\Delta\psi$. **b,d,f,** The ΔT results from the panels **a**, **c**, and **e** calculated for a range of ψ_s with line thickness proportional to parameters in the aforementioned panels (e.g., thick blue line in panel **b** corresponds to 50% increase in g_{sp} shown in panel **a**). The x-axes are mapped from ψ_l in the top panels to ψ_s in the bottom panels.~~

3.3 Improving Transpiration Predictions with a PHM and a 'Dynamic β'

We now ~~examine the divergence between PHMs and~~ perform a modeling case study of the Ameriflux US-Me2 ponderosa site (Sect. 2.4) using our own calibrated LSM (Sect. 2.3) with five separate transpiration downregulation schemes: i) well-watered (no downregulation), ii) single β ~~for a real transport-limited soil-plant system. We calibrated our own land surface model (LSM (β_s), iii) β separately applied to sunlit and shaded leaf areas (β_{2L}), iv) β_{dyn}, and v) PHM. Specifically we aim to i) mirroring CLM v5 (Oleson et al., 2018) (section S6 of the Supplement)to the surface energy budget and gross primary productivity (GPP)data at the Ameriflux Metolius ponderosa pine site in Oregon, USA (US-Me2 (Irvine et al., 2008)) for May-August 2013-2014. We use the calibrated LSM to (i) explore the spectrum of~~ validate the transport-limitation ~~in a realistic system, (ii) quantify~~ spectrum (Sect. 3.1) for a more complex PHM formulation common to TBMs, ii) identify errors incurred by selecting β over a PHM ~~, and ((~~Sect. 3.2) for a real transport-limited soil-plant system, and iii) develop ~~and test~~ a new 'dynamic β' that approximates ~~the behaviors of the PHM with two additional parameters to the original~~ a PHM with simple modifications to the existing β~~function~~.

To aid our comparison of LSM transpiration downregulation schemes, we must first verify that the spectrum of transport-limitation found in our minimalist analysis (Sect. 3.1) adequately describes the differences between PHMs and the β formulations common to TBMs. Our calibrated LSM uses a more complex ~~formulation of the PHM common to TBMs (Bonan et al., 2014; Kennedy et al~~ ~~and ecohydrological models (Sperry et al., 1998; Manzoni et al., 2014)~~ PHM formulation (Sect. 2.2 and Fig. 1b) that partitions

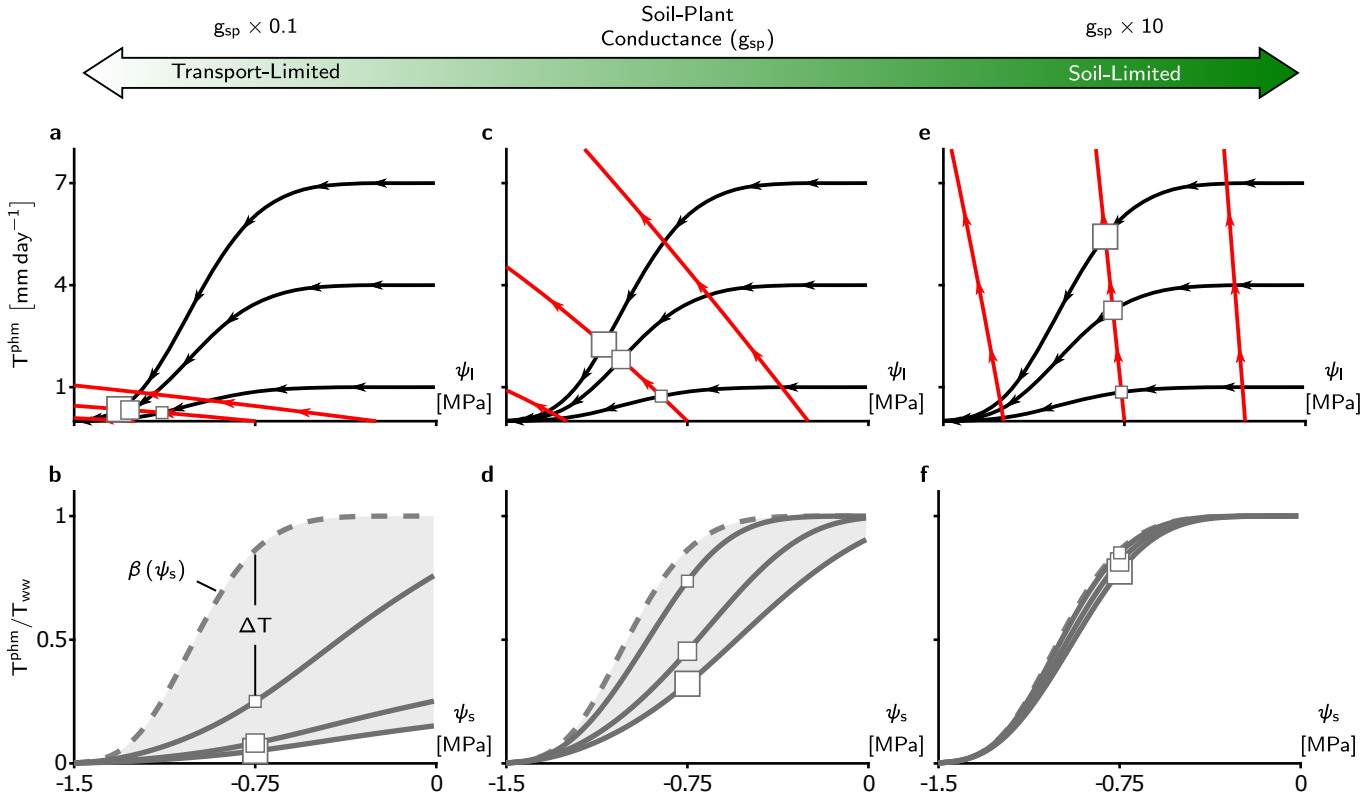

Figure 4. Transport-limitation spectrum observed in complex PHM formulation. **a,c,e,** Supply-demand curves for three values of soil-plant conductance, g_{sp}, using the more complex PHM formulation. Panel **c** is based on calibrated parameters ($g_{sp} \approx 13\,\mathrm{mm\,day^{-1}\,MPa^{-1}}$) from the US-Me2 Ameriflux site containing mature ponderosa pines that were determined for the LSM analysis in this paper. Panels **a** and **e** contains the calibrated g_{sp} multiplied by 0.1 and 10, respectively. The supply lines (red) are shown at ψ_s equal to 0, ~~-7.5~~ -0.75, and ~~-15 MPa~~ -1.5 MPa and demand lines (black) are shown at T_{ww} equal to ~~30~~1, ~~90~~4, and ~~150 W m^{-2}~~7 $\mathrm{mm\,day^{-1}}$. The PHM solution for ψ_s at ~~-7.5~~ -0.75 MPa is shown by the squares with size corresponding to T_{ww} magnitude. **b,d,f,** The relative transpiration for the PHM (solid) in panels **a**, **c**, and **e** and the infinitely conductive β solution (dashed line).

the soil-plant-atmosphere continuum into soil-to-xylem, xylem-to-leaf, and leaf-to-atmosphere segments, ~~and uses nonlinear~~ each with conductance curves that depend nonlinearly (e.g., sigmoidal or Weibull) ~~functions to represent downregulation of segment-specific conductances (Eq. 6-11).~~ on water potential. This added complexity does not affect the ~~the~~ spectrum of transport-limitation ~~found in the minimalist PHM, shown for the calibrated LSM in an analogous supply-demand framework in~~ (Fig. 4). For clarity, we reiterate two main points from the minimalist PHM analysis found in this complex analysis. ~~Two main points are worth reiterating.~~ First, soil-plant conductance (g_{sp}) controls whether the soil-plant system is ~~supply-limited~~ soil-limited (high g_{sp}; Fig. 4e-f) or transport-limited (low g_{sp}; Fig. 4a-b) due to non-negligible water potential differences ($\Delta\psi$) ~~, resulting in~~ creating large differences between PHMs and β (high ΔT) at intermediate ψ_s values (Fig. 4b,d). Second, for a transport-limited system, ΔT increases with higher variability in atmospheric moisture demand (T_{ww}~~. To elaborate on~~

this second point, we note that the plotted), where the importance of 'variability' expands on our minimalist results. To clarify, β function is shown in this case as an upper bound of transport-limited behavior (as $g_{sp} \to \infty$). However, in practice, β is should be considered an empirical model ; depending on how the modeler chooses to fit the β function, it could exist that could be fit anywhere within the range of the PHM downregulation envelope . Therefore, we must emphasize that the larger range of T_{ww} results in a greater range of downregulation behaviors from the PHM ((light gray shading in Fig. 4b), making a ,d,f). Therefore, greater T_{ww} variability creates a larger PHM downregulation envelope and makes a single β increasingly inadequate for capturing the range of behaviors within this downregulationenvelope. The consistency in the results based on the minimalist and the modeling transpiration downregulation.

The consistency between the minimalist and more complex PHM suggests that the divergence between PHMs and β in transport-limited systems is not contingent on are not sensitive to the linear or nonlinear forms of supply or demand lines, but rather on are rather controlled by the existence of a finite conductance itself. Furthermore, these results strongly support the need to use two independent variables, ψ_s and T_{ww} (rather than only ψ_s in β), to capture the coupled effects of soil water stress and atmospheric moisture demand on transpiration downregulation when in transport-limited soil-plant systemsare transport-limited.

LSM evapotranspiration estimates improved by PHM and new 'dynamic β'. **a-b**, Fits of the β_s, β_{2L}, and β_{dyn} schemes to the relative transpiration outputs from the calibrated PHM scheme for the sunlit (**a**) and shaded big leaf (**b**) of the LSM (see Methods). Note that only three of the infinite family of β_{dyn} curves are shown for illustration. Full fitting details of these three schemes are available in section S2 of the Supplement. **c-d**, The median diurnal ET estimates for the LSM with five transpiration downregulation schemes compared to Ameriflux observations at the US-Me2 site for early (**c**) and late summer (**d**). The dual source LSM calculates ET as the sum of sunlit and shaded big leaf transpiration and ground evaporation. Note: β_{dyn} (red) is overlying PHM (black) results as they are essentially the same. **e-f**, Reduction in absolute percent bias between the β_s and PHM schemes (**e**) and β_{dyn} and PHM schemes (**f**) in terms of atmospheric moisture demand (represented by T_{ww}) and soil water status (represented by θ_s). In both plots, blue indicates PHM improvement over the selected β scheme.

. In light of these findings, we have developed a new 'dynamic β' (β_{dyn}) that has an additional functional dependence on T_{ww} (Eq. 16) and compared it against four other downregulation schemes in this LSM analysis. Thus, the LSM was run using a total of five different transpiration downregulation schemes: 1) well-watered (no downregulation), 2) single β (β_s), 3) β separately applied to sunlit and shaded leaf areas (β_{2L}), 4) β_{dyn}, and 5) PHM . The LSM with PHM scheme was calibrated to the Ameriflux data while the β schemes were each fit to the calibrated relative transpiration outputs (T^{phm}/T_{ww}) that vary with both ψ_s and T_{ww} as previously suggested (Fig. 5a-b). We refer the reader to the Sect. 2.3 for calibration and fitting details.

We now assess the errors incurred by using a β rather than PHM downregulation scheme to model the US-Me2 ponderosa pine site. The median diurnal evapotranspiration (ET) from each LSM is compared to the Ameriflux data for early and late ; bare soil evaporation plus transpiration) for each LSM version for early summer 2013-2014 (Fig. 5c-d) . During early summer, all models indicates that all downregulation schemes perform similarly due to high soil moisture and minimal downregulation (Fig. 5c). During late summer, However, as soil moisture declines during late summer (Fig. S1 of the Supplement) , and

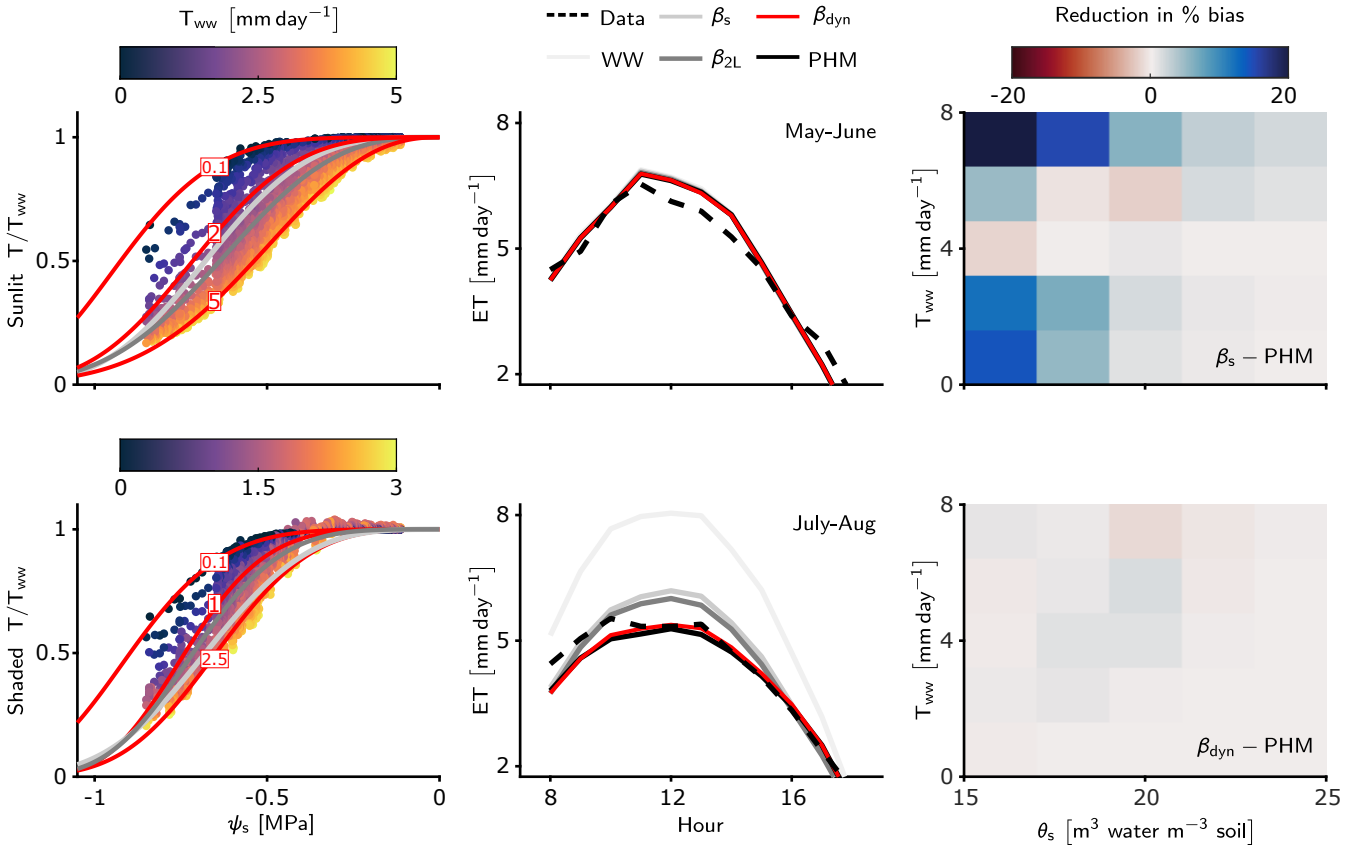

Figure 5. LSM evapotranspiration estimates improved by PHM and new 'dynamic β'. **a-b**, Fits of the β_s, β_{2L}, and β_{dyn} schemes to the relative transpiration outputs from the calibrated PHM scheme for the sunlit (**a**) and shaded big-leaf (**b**) of the LSM (see Methods). Note that only three of the infinite family of β_{dyn} curves are shown for illustration. Full fitting details of these three schemes are available in Sect. S2. **c-d**, The median diurnal ET estimates for the LSM with five transpiration downregulation schemes compared to Ameriflux observations at the US-Me2 site for early (**c**) and late summer (**d**). The dual source LSM calculates ET as the sum of sunlit and shaded big-leaf transpiration and ground evaporation. Note: β_{dyn} (red) is overlying PHM (black) results as they are essentially the same. **e-f**, Reduction in absolute percent bias of ET between the β_s and PHM schemes (**e**) and β_{dyn} and PHM schemes (**f**) in terms of atmospheric moisture demand (represented by T_{ww}) and soil water status (represented by θ_s). In both plots, blue indicates PHM improvement over the selected β scheme.

~~differences between downregulation schemes emerge. The~~ S11) the differences between schemes emerge: the PHM and β_{dyn} schemes fit the ET observations the best, while β_{2L}, β_s, and well-watered schemes over-predict ET (Fig. 5d). ~~The sources of bias for~~ We explain the poor performance of the static β schemes ~~are illustrated~~ by plotting the reduction in absolute percent bias between the β_s and PHM schemes (Fig. 5e) ~~for a range of soil~~ of soil water stress (represented by volumetric soil water content ~~,~~ measurements at the site (θ_s [$\mathrm{m^3}$ water $\mathrm{m^{-3}}$ soil])) and atmospheric moisture ~~conditions~~ demand (represented by T_{ww} from the well-watered LSM version). The PHM scheme provides substantial percent bias reduction relative to the static β_s scheme under soil water stress ($\theta_s < 0.2$) for above- and below-average T_{ww} values (~~$T_{ww} \approx 120\,\mathrm{W\,m^{-2}}$~~ $T_{ww} \approx 4\,\mathrm{mm\,day^{-1}}$).

This result is true for both static β schemes (β_s and β_{2L}) because they are fit to the average T_{ww} ~~at each ψ_s~~ behavior over the simulation period (Fig. 5a-b and Sect. S6.2). Therefore, as T_{ww} becomes higher (lower) than the average, these static β schemes will overpredict (underpredict) transpiration. The PHM also improves performance during wetter soil conditions ($\theta_s > 0.2$) with high T_{ww}—which do not represent typical 'drought' conditions—suggesting that PHMs ~~are more appropriate than~~ capture transpiration downregulation that β ~~for representing transpiration downregulation caused by~~ potentially misses as it cannot account for large soil-plant potential differences ($\Delta\psi$) under transport-limitation and/or high atmospheric moisture demand ~~.~~ (similar to Sect. 3.2). Lastly, the near average T_{ww} conditions lead to β providing enhanced performance, which can be explained by underlying biases in the calibrated parameter estimates (see Fig. ~~S10 of the Supplement~~S9).

Notably, the β_{dyn} downregulation scheme replicates the performance of the PHM scheme by adding a single dimension of T_{ww} to the original β scheme. ~~The difference in performance~~ This additional dependence on T_{ww} allows β_{dyn} to traverse along the PHM downregulation envelope with atmospheric moisture demand changes, whereas the static β schemes are fixed near mean conditions (Fig. 5a-b). The performance difference between PHM and β_{dyn} schemes is minimal in terms of percent change in bias across all environmental conditions (Fig. 5f), median diurnal variations (Fig. 5~~a-b~~c-d), and cumulative flux errors (Table ~~S1 of the Supplement~~S7-S8). Therefore, this additional dependence on T_{ww} is key to simulating the coupled effects of atmospheric moisture demand and soil water stress in PHMs and accurately modeling transpiration downregulation in transport-limited systems. For this transport-limited system, β_{dyn} requires two more parameters than the original β scheme, which is half the parameters required for our complex PHM formulation (Sect. S6.2). Furthermore, β_{dyn} does not require the iterative solution of water potentials and transpiration in PHMs (Sect. 2.2). Rather, it calculates transpiration downregulation algebraically using ψ_s as in the original β. The β_{dyn} provides a future avenue for correcting existing β model bias without adding the computational and parametric challenges of more realistic PHMs.

4 Discussion and Conclusion

The spectrum of transport-limited transpiration ~~highlighted in this work~~ explains why many TBMs that use β to represent transpiration downregulation struggle to predict water, energy, and carbon fluxes under soil water stress (Sitch et al., 2008; Powell et al., 2013; Medlyn et al., 2016; Ukkola et al., 2016; Restrepo-Coupe et al., 2017; Trugman et al., 2018) and why implementing PHMs has led to performance improvements (Kennedy et al., 2019; Anderegg and Venturas, 2020; Eller et al., 2020; Sabot et al., 2020). ~~A~~ Transpiration in a transport-limited soil-plant system, characterized by finite soil-plant conductance, ~~leads to a~~ depends on non-negligible water potential ~~difference between the soil and the leaf~~differences to transport water from the soil to the leaf, which results from the joint effects of atmospheric moisture demand and soil water supply on leaf water potential. It is only when the soil-plant conductance becomes infinite (and the system becomes ~~supply-limited~~soil-limited) that leaf water potential approximates soil water potential, and transpiration arises as an independent function of soil water supply and atmospheric moisture demand. These are assumptions inherent to the empirical β and explains why β cannot capture the coupled effects of soil water stress and atmospheric moisture demand.

The implications of continued use of β will vary by site. Ecosystems with soil or plant hydraulic properties resistant to flow (e.g., xeric ecosystems, tall trees, species with low xylem conductivity or roots that hydraulically disconnects from the soil during drought) will have large biases depending on the range of soil water availability and atmospheric moisture demand (T_{ww}) observed at the site (Fig. 3d and 4b). These errors will not be confined to drought periods, ~~and will also occur~~ as higher atmospheric moisture demand and lower soil-plant conductance can result in errors even during wetter soil conditions (~~low soil water stress) when atmospheric moisture demand is high (~~Fig. 3 and Fig. 5e). This is a crucial point, given ~~that ecosystems are projected to experience~~ projections indicate diverging degrees of VPD stress and soil water stress ~~in the future~~ for ecosystems (Novick et al., 2016). On the other hand, for ~~supply-limited~~ soil-limited systems (e.g., ~~riparian vegetation,~~ irrigated crops, riparian vegetation, or groundwater-dependent ecosystems), β may adequately capture transpiration dynamics as soil water status may be a suitable proxy for leaf water status. Therefore, ~~identifying~~ further work must identify the combinations of soil parameters and plant hydraulic traits that define transport- or ~~supply-limited systems is an important future step for locating areas around the globe susceptible to prediction error~~soil-limited systems to identify ecosystems susceptible to bias from β. Our initial estimates indicate a ~~value of~~ soil-plant conductance ~~around 10^3 may act as~~ value around 30 $\mathrm{mm\,day^{-1}\,MPa^{-1}}$ may be a rough threshold for transport-limitation (see ~~section S3 of the Supplement) .~~ Sect. S7).

Several other factors not covered in this work could exacerbate the differences between β and PHM predictions. We expect plant capacitance (already incorporated into some TBMs (Xu et al., 2016; Christoffersen et al., 2016)) will likely cause further deviations from β. PHMs with capacitance is expected to introduce hysteresis into transpiration downregulation (Zhang et al., 2014) in transport-limited systems that existing β are not equipped to capture. However, this hysteretic behavior may diminish in a high conductance (i.e., soil-limited) system because plant and soil water potentials will quickly equilibrate, so β may still be an adequate alternative to a PHM. More advanced representation of stomatal response and plant hydraulic transport could further exacerbate β and PHM differences. Recent advances in optimality-based (Eller et al., 2020; Sabot et al., 2020) and mechanistic stomatal response models (Buckley, 2017) as well as more detailed PHM segmentation (Kennedy et al., 2019) may include additional couplings to plant water and metabolism that cannot be easily approximated by β. Regardless, the core message of this work is still relevant: for transport-limited soil-plant systems, PHMs are necessary to couple the effects of soil water stress and atmospheric moisture demand on transpiration, and β fails because soil water status is not an adequate substitute for leaf water status.

The recognition that a 'dynamic β' model can replicate the complexity of a PHM with half the parameters and more direct computation (~~see section S2~~Sect. S6.2~~of the Supplement~~), simply by adding a dependence on atmospheric moisture demand to the β function, provides a useful pathway for overcoming both the limitations of β and the parametric uncertainties of PHMs (Paschalis et al., 2020; Anderegg and Venturas, 2020). The inadequacies of the static β have been noted since its inception. Feddes et al. (1978), who introduced the first β, mentioned β's dependence on atmospheric moisture demand based on field data (Denmead and Shaw, 1962; Yang and de Jong, 1972) and early plant hydraulic theory (Gardner, 1960). Unfortunately, there have been only a few attempts to rectify these inadequacies in the modeling community, short of implementing a full PHM. For example, Feddes and Raats (2004) updated their original β model to vary the water potential at incipient stomatal closure linearly with atmospheric moisture demand, which has been adopted in the field scale SWAP model (Kroes et al., 2017),

while the Ecosystem Demography-2 model (Medvigy et al., 2009) uses a sigmoidal function for transpiration downregulation that contains the ratio of soil water supply to evaporative demand. Within many TBMs and hydrological models, a 'dynamic β' could easily replace the original β by allowing existing fixed parameters to vary with T_{ww} (already calculated in many transpiration downregulation schemes). ~~This would offer a physically-informed alternative to PHMs, with a simpler calibration process.~~ In addition to improving TBM performances, 'dynamic β' also has the potential to aid in remote sensing retrievals and indirect inferences of land surface fluxes. Currently, the state-of-the-art ECOSTRESS satellite provides global ET estimates based on a modified Priestley-Taylor formulation that uses a β function to downregulate ET under soil water stress (Fisher et al., 2020). These satellite products could easily implement the 'dynamic β' formulation to correct biases for many transport-limited ecosystems. These potential applications rely on formalizing the relationship between the 'dynamic β' parameters and their dependence on T_{ww}. As it stands, the 'dynamic β' still needs to be calibrated to site-specific data; however, it provides a physically-informed alternative to PHMs with less calculation and fewer parameters. Further work will focus on ~~linking these relationships~~ generalizing the 'dynamic β' by linking its parameters to measurable soil properties, plant hydraulic traits, and atmospheric feedbacks.

Code availability.

Author contributions. X.F. and S.T. conceived the idea; B.P.S and X.F. designed the research; B.P.S. performed the research; B.P.S. and X.F. wrote the paper; and S.T. contributed to refining results and revising the paper.

Competing interests. The authors declare no competing interests.

Acknowledgements. ~~The authors have no acknowledgements to make~~B.P.S. and X.F. acknowledge support from National Science Foundation award DEB-2045610. B.P.S. and X.F. also acknowledge the resources from The Minnesota Supercomputing Institute used to run the simulations in this work.

References

Anderegg, W. R., Wolf, A., Arango-Velez, A., Choat, B., Chmura, D. J., Jansen, S., Kolb, T., Li, S., Meinzer, F., Pita, P., Resco de Dios, V., Sperry, J. S., Wolfe, B. T., and Pacala, S.: Plant water potential improves prediction of empirical stomatal models, PLoS ONE, 12, 1–17, , 2017.

Anderegg, W. R. L.: Minireview Spatial and temporal variation in plant hydraulic traits and their relevance for climate change impacts on vegetation, New Phytologist, 205, 1008–1014, https://doi.org/10.1111/nph.12907, www.newphytologist.com, 2015.

Anderegg, W. R. L. and Venturas, M. D.: Plant hydraulics play a critical role in Earth system fluxes, New Phytologist, N/A, 4, https://doi.org/10.1111/nph.16548, http://doi.wiley.com/10.1111/nph.16548, 2020.

Bohrer, G., Mourad, H., Laursen, T. A., Drewry, D., Avissar, R., Poggi, D., Oren, R., Katul, G. G., Bohrer, C. ., Mourad, H., Laursen, T. A., Drewry, D., Avissar, R., Poggi, D., Oren, R., and Katul, G. G.: Finite element tree crown hydrodynamics model (FETCH) using porous media flow within branching elements: A new representation of tree hydrodynamics, 41, 11 404, https://doi.org/10.1029/2005WR004181, 2005.

Bonan, G.: Climate Change and Terrestrial Ecosystem Modeling, Cambridge University Press, https://doi.org/10.1017/9781107339217, https://www.cambridge.org/core/product/identifier/9781107339217/type/book, 2019.

Bonan, G. B., Williams, M., Fisher, R. A., and Oleson, K. W.: Modeling stomatal conductance in the earth system: linking leaf water-use efficiency and water transport along the soil–plant–atmosphere continuum, Geoscientific Model Development, 7, 2193–2222, https://doi.org/10.5194/gmd-7-2193-2014, https://www.geosci-model-dev.net/7/2193/2014/, 2014.

Buckley, T. N.and Mott, K. A: Modeling Stomatal Conductance, Plant Physiology, 174, 572–582, https://doi.org/10.1104/pp.16.01772, www.plantphysiol.org/cgi/doi/10.1104/pp.16.01772, 2017.

Buckley, T. N.: Modelling stomatal conductance in response to environmental factorsHow do stomata respond to water status?, Plant, Cell and Environment, 36, 1691–1699, , New Phytologist, 224, 21–36, https://doi.org/10.1111/nph.15899, , 2013. https://onlinelibrary.wiley.com/doi/abs/10.1111/nph.15899, 2019.

Buckley, T. N., Martorell, S., Diaz-Espejo, A., Tomàs, M., and Medrano, H.: Is stomatal conductance optimized over both time and space in plant crowns? A field test in grapevine (Vitis vinifera), https://doi.org/10.1111/pce.12343, https://onlinelibrary.wiley.com/doi/pdf/10.1111/pce.12343, 2014.

Christoffersen, B. O., Gloor, M., Fauset, S., Fyllas, N. M., Galbraith, D. R., Baker, T. R., Kruijt, B., Rowland, L., Fisher, R. A., Binks, O. J., Sevanto, S., Xu, C., Jansen, S., Choat, B., Mencuccini, M., McDowell, N. G., and Meir, P.: Linking hydraulic traits to tropical forest function in a size-structured and trait-driven model (TFS v.1-Hydro), Geoscientific Model Development, 9, 4227–4255, https://doi.org/10.5194/gmd-9-4227-2016, https://www.geosci-model-dev.net/9/4227/2016/, 2016.

Clapp, R. B. and Hornberger, G. M.: Empirical equations for some soil hydraulic properties, Water Resources Research, 14, 601–604, https://doi.org/10.1029/WR014i004p00601, http://doi.wiley.com/10.1029/WR014i004p00601, 1978.

Collatz, G., Ball, J., Grivet, C., and Berry, J. A.: Physiological and environmental regulation of stomatal conductance, photosynthesis and transpiration: a model that includes a laminar boundary layer, Agricultural and Forest Meteorology, 54, 107–136, https://doi.org/10.1016/0168-1923(91)90002-8, https://www.sciencedirect.com/science/article/pii/0168192391900028, 1991.

Couvreur, V., Ledder, G., Manzoni, S., Way, D. A., Muller, E. B., and Russo, S. E.: Water transport through tall trees: A vertically explicit, analytical model of xylem hydraulic conductance in stems, Plant, Cell & Environment, 41, 1821–1839, https://doi.org/10.1111/pce.13322, http://doi.wiley.com/10.1111/pce.13322, 2018.

Cowan, I. R.: Transport of Water in the Soil-Plant-Atmosphere System, Tech. Rep. 1, 1965.

Daly, E., Porporato, A., Rodriguez-Iturbe, I., Daly, E., Porporato, A., and Rodriguez-Iturbe, I.: Coupled Dynamics of Photosynthesis, Transpiration, and Soil Water Balance. Part I: Upscaling from Hourly to Daily Level, Journal of Hydrometeorology, 5, 546–558, https://doi.org/10.1175/1525-7541(2004)005<0546:CDOPTA>2.0.CO;2, http://journals.ametsoc.org/doi/abs/10.1175/1525-7541%282004%29005%3C0546%3ACDOPTA%3E2.0.CO%3B2, 2004.

Damour, G., Simonneau, T., Cochard, H., and Urban, L.: An overview of models of stomatal conductance at the leaf level, Plant, Cell and Environment, 33, 1419–1438, https://doi.org/10.1111/j.1365-3040.2010.02181.x, 2010.

De Kauwe, M. G., Zhou, S.-X., Medlyn, B. E., Pitman, A. J., Wang, Y.-P., Duursma, R. A., and Prentice, I. C.: Do land surface models need to include differential plant species responses to drought? Examining model predictions across a mesic-xeric gradient in Europe, Biogeosciences, 12, 7503–7518, https://doi.org/10.5194/bg-12-7503-2015, www.biogeosciences.net/12/7503/2015/, 2015.

DeLucia, E. H. and Heckathorn, S. A.: The effect of soil drought on water-use efficiency in a contrasting Great Basin desert and Sierran montane species, Plant, Cell & Environment, 12, 935–940, https://doi.org/10.1111/j.1365-3040.1989.tb01973.x, 1989.

Denmead, O. T. and Shaw, R. H.: Availability of Soil Water to Plants as Affected by Soil Moisture Content and Meteorological Conditions 1, Agronomy Journal, 54, 385–390, https://doi.org/10.2134/agronj1962.00021962005400050005x, http://doi.wiley.com/10.2134/agronj1962.00021962005400050005x, 1962.

Egea, G., Verhoef, A., and Vidale, P. L.: Towards an improved and more flexible representation of water stress in coupled photosynthesis–stomatal conductance models, Agricultural and Forest Meteorology, 151, 1370–1384, https://doi.org/10.1016/J.AGRFORMET.2011.05.019, https://www.sciencedirect.com/science/article/pii/S0168192311001778, 2011.

Eller, C. B., Rowland, L., Mencuccini, M., Rosas, T., Williams, K., Harper, A., Medlyn, B. E., Wagner, Y., Klein, T., Teodoro, G. S., Oliveira, R. S., Matos, I. S., Rosado, B. H. P., Fuchs, K., Wohlfahrt, G., Montagnani, L., Meir, P., Sitch, S., and Cox, P. M.: Stomatal optimization based on xylem hydraulics (SOX) improves land surface model simulation of vegetation responses to climate, New Phytologist, N/A, 1–16, https://doi.org/10.1111/nph.16419, https://onlinelibrary.wiley.com/doi/abs/10.1111/nph.16419, 2020.

Farquhar, G. D., von Caemmerer, S., and Berry, J. A.: A biochemical model of photosynthetic CO2 assimilation in leaves of C3 species, Planta, https://doi.org/10.1007/BF00386231, 1980.

Fatichi, S., Pappas, C., and Ivanov, V. Y.: Modeling plant-water interactions: an ecohydrological overview from the cell to the global scale, Wiley Interdisciplinary Reviews: Water, 3, 327–368, https://doi.org/10.1002/wat2.1125, http://doi.wiley.com/10.1002/wat2.1125, 2016.

Feddes, R. A. and Raats, P. C.: Parameterizing the soil - water - plant root system, in: Unsaturated-zone modeling: Progress, challenges and applications, chap. 4, pp. 95–141, Kluwer Academic Publishers, Dordrecht, 2004.

Feddes, R. A., Kowalik, P. J., and Zaradny, H.: Simulation of field water use and crop yield. Simulation monographs, Halsted Press, Wageningen, 1978.

Feng, X.: Marching in step: The importance of matching model complexity to data availability in terrestrial biosphere models, Global Change Biology, 26, 3190–3192, https://doi.org/10.1111/gcb.15090, https://onlinelibrary.wiley.com/doi/abs/10.1111/gcb.15090, 2020.

Feng, X., Ackerly, D. D., Dawson, T. E., Manzoni, S., Skelton, R. P., Vico, G., and Thompson, S. E.: The ecohydrological context of drought and classification of plant responses, Ecology Letters, N/A, 14, https://doi.org/10.1111/ele.13139, 2018.

Fisher, J. B., Lee, B., Purdy, A. J., Halverson, G. H., Dohlen, M. B., Cawse-Nicholson, K., Wang, A., Anderson, R. G., Aragon, B., Arain, M. A., Baldocchi, D. D., Baker, J. M., Barral, H., Bernacchi, C. J., Bernhofer, C., Biraud, S. C., Bohrer, G., Brunsell, N., Cappelaere, B., Castro-Contreras, S., Chun, J., Conrad, B. J., Cremonese, E., Demarty, J., Desai, A. R., De Ligne, A., Foltýnová, L., Goulden, M. L., Griffis, T. J., Grünwald, T., Johnson, M. S., Kang, M., Kelbe, D., Kowalska, N., Lim, J.-H., Maïnassara, I., Mccabe, M. F., Missik, J. E. C., Mohanty, B. P., Moore, C. E., Morillas, L., Morrison, R., Munger, J. W., Posse, G., Richardson, A. D., Russell, E. S., Ryu, Y., Sanchez-Azofeifa, A., Schmidt, M., Schwartz, E., Sharp, I., Šigut, L., Tang, Y., Hulley, G., Anderson, M., Hain, C., French, A., Wood, E., Hook, S., Fisher, J. B., Lee, B., Purdy, A. J., Halverson, G. H., Dohlen, M. B., and Fisher, A. L.: ECOSTRESS: NASA's Next Generation Mission to Measure Evapotranspiration From the International Space Station, Water Resources Research, 56, https://doi.org/10.1029/2019WR026058, https://doi.org/, 2020.

Fisher, R. A., Koven, C. D., Anderegg, W. R., Christoffersen, B. O., Dietze, M. C., Farrior, C. E., Holm, J. A., Hurtt, G. C., Knox, R. G., Lawrence, P. J., Lichstein, J. W., Longo, M., Matheny, A. M., Medvigy, D., Muller-Landau, H. C., Powell, T. L., Serbin, S. P., Sato, H., Shuman, J. K., Smith, B., Trugman, A. T., Viskari, T., Verbeeck, H., Weng, E., Xu, C., Xu, X., Zhang, T., and Moorcroft, P. R.: Vegetation demographics in Earth System Models: A review of progress and priorities, https://doi.org/10.1111/gcb.13910, https://onlinelibrary-wiley-com.ezp1.lib.umn.edu/doi/full/10.1111/gcb.13910https://onlinelibrary-wiley-com.ezp1.lib.umn.edu/doi/abs/10.1111/gcb.13910https://onlinelibrary-wiley-com.ezp1.lib.umn.edu/doi/10.1111/gcb.13910, 2018.

Franks, S. J., Weber, J. J., and Aitken, S. N.: Evolutionary and plastic responses to climate change in terrestrial plant populations, Evolutionary Applications, 7, 123–139, https://doi.org/10.1111/eva.12112, https://onlinelibrary.wiley.com/doi/10.1111/eva.12112, 2014.

Gardner, W. R.: Dynamic aspects of water availability to plants, Soil Science, 89, 63–73, https://doi.org/10.1097/00010694-196002000-00001, 1960.

Goudriaan, J. and Laar, H. H. v.: Modelling potential crop growth processes : textbook with exercises, https://doi.org/10.1007/978-94-011-0750-1, 1994.

Irvine, J., Law, B. E., Martin, J. G., and Vickers, D.: Interannual variation in soil CO2 efflux and the response of root respiration to climate and canopy gas exchange in mature ponderosa pine, Global Change Biology, 14, 2848–2859, https://doi.org/10.1111/j.1365-2486.2008.01682.x, 2008.

Jarvis, P.: The interpretation of the variations in leaf water potential and stomatal conductance found in canopies in the field, Tech. rep., 1976.

Katul, G. G., Oren, R., Manzoni, S., Higgins, C., and Parlange, M. B.: Evapotranspiration: A process driving mass transport and energy exchange in the soil-plant-atmosphere-climate system, https://doi.org/10.1029/2011RG000366, 2012.

Kennedy, D., Swenson, S., Oleson, K. W., Lawrence, D. M., Fisher, R., Lola da Costa, A. C., and Gentine, P.: Implementing Plant Hydraulics in the Community Land Model, Version 5, Journal of Advances in Modeling Earth Systems, 11, 485–513, https://doi.org/10.1029/2018MS001500, http://doi.wiley.com/10.1029/2018MS001500, 2019.

Klein, T.: The variability of stomatal sensitivity to leaf water potential across tree species indicates a continuum between isohydric and anisohydric behaviours, Functional Ecology, 28, 1313–1320, https://doi.org/10.1111/1365-2435.12289, http://doi.wiley.com/10.1111/1365-2435.12289, 2014.

Kowalczyk, E. A., Wang, Y. P., Law, R. M., Davies, H. L., Mcgregor, J. L., and Abramowitz, G.: The CSIRO Atmosphere Biosphere Land Exchange (CABLE) model for use in climate models and as an offline model, Tech. rep., http://www.cmar.csiro.au/e-print/open/kowalczykea_2006a.pdf, 2006.

Kroes, J. G., van Dam, J., Bartholomeus, R., Groenendijk, P., Heinen, M., Hendriks, R., Mulder, H., Supit, I., and van Walsum, P.: SWAP version 4: Theory description and user manual, Tech. rep., Wageningen Environmental Research, Wageningen, https://doi.org/ISSN 1566-7197, 2017.

Lin, C., Gentine, P., Huang, Y., Guan, K., Kimm, H., and Zhou, S.: Diel ecosystem conductance response to vapor pressure deficit is suboptimal and independent of soil moisture, Agricultural and Forest Meteorology, 250-251, 24–34, https://doi.org/10.1016/J.AGRFORMET.2017.12.078, https://www.sciencedirect.com/science/article/pii/S0168192317304884, 2018.

Liu, Y., Kumar, M., Katul, G. G., Feng, X., and Konings, A. G.: Plant hydraulics accentuates the effect of atmospheric moisture stress on transpiration, Nature Climate Change, 10, 691–695, https://doi.org/10.1038/s41558-020-0781-5, https://doi.org/10.1038/s41558-020-0781-5, 2020.

~~Manzoni, S., Vico, G., Katul, G., Palmroth, S., and Porporato, A.: Optimal plant water-use strategies under stochastic rainfall, Water Resources Research, 50, 1–16, , 2014.~~

~~McAdam, S. A. M. and Brodribb, T. J.: Linking Turgor with ABA Biosynthesis: Implications for Stomatal Responses to Vapor Pressure Deficit across Land Plants., Plant physiology, 171, 2008–16, , , 2016.~~

Medlyn, B. E., Duursma, R. A., Eamus, D., Ellsworth, D. S., Prentice, I. C., Barton, C. V. M., Crous, K. Y., De Angelis, P., FREEMAN, M., and WINGATE, L.: Reconciling the optimal and empirical approaches to modelling stomatal conductance, Global Change Biology, 17, 2134–2144, https://doi.org/10.1111/j.1365-2486.2010.02375.x, http://doi.wiley.com/10.1111/j.1365-2486.2010.02375.x, 2011.

Medlyn, B. E., De Kauwe, M. G., Zaehle, S., Walker, A. P., Duursma, R. A., Luus, K., Mishurov, M., Pak, B., Smith, B., Wang, Y.-P., Yang, X., Crous, K. Y., Drake, J. E., Gimeno, T. E., Macdonald, C. A., Norby, R. J., Power, S. A., Tjoelker, M. G., and Ellsworth, D. S.: Using models to guide field experiments: a priori predictions for the CO 2 response of a nutrient- and water-limited native Eucalypt woodland, Global Change Biology, 22, 2834–2851, https://doi.org/10.1111/gcb.13268, http://doi.wiley.com/10.1111/gcb.13268, 2016.

Medvigy, D., Wofsy, S. C., Munger, J. W., Hollinger, D. Y., and Moorcroft, P. R.: Mechanistic scaling of ecosystem function and dynamics in space and time: Ecosystem Demography model version 2, Journal of Geophysical Research: Biogeosciences, 114, G01 002, https://doi.org/10.1029/2008JG000812, http://doi.wiley.com/10.1029/2008JG000812, 2009.

Mencuccini, M., Manzoni, S., and Christoffersen, B. O.: Modelling water fluxes in plants: from tissues to biosphere, New Phytologist, https://doi.org/10.1111/nph.15681, 2019.

Novick, K. A., Ficklin, D. L., Stoy, P. C., Williams, C. A., Bohrer, G., Oishi, A. C., Papuga, S. A., Blanken, P. D., Noormets, A., Sulman, B. N., Scott, R. L., Wang, L., and Phillips, R. P.: The increasing importance of atmospheric demand for ecosystem water and carbon fluxes, Nature Climate Change, 6, 1023–1027, https://doi.org/10.1038/nclimate3114, 2016.

Oleson, K. W., Lead, D. M. L., Bonan, G. B., Drewniak, B., Huang, M., Koven, C. D., Levis, S., Li, F., Riley, W. J., Subin, Z. M., Swenson, S. C., Thornton, P. E., Bozbiyik, A., Fisher, R., Heald, C. L., Kluzek, E., Lamarque, J.-F., Lawrence, P. J., Leung, L. R., Lipscomb, W., Muszala, S., Ricciuto, D. M., Sacks, W., Sun, Y., Tang, J., and Yang, Z.-L.: Technical Description of the version 5.0 of the Community Land Model (CLM), Tech. rep., http://www.cesm.ucar.edu/models/cesm2/land/CLM50_Tech_Note.pdfhttp://library.ucar.edu/research/publish-technote, 2018.

Pammenter, N. W. and Willigen, C. V.: A mathematical and statistical analysis of the curves illustrating vulnerability of xylem to cavitation, in: Tree Physiology, https://doi.org/10.1093/treephys/18.8-9.589, 1998.

Paschalis, A., Fatichi, S., Zscheischler, J., Ciais, P., Bahn, M., Boysen, L., Chang, J., De Kauwe, M., Estiarte, M., Goll, D., Hanson, P. J., Harper, A. B., Hou, E., Kigel, J., Knapp, A. K., Larsen, K. S., Li, W., Lienert, S., Luo, Y., Meir, P., Nabel, J. E., Ogaya, R., Parolari, A. J., Peng, C., Peñuelas, J., Pongratz, J., Rambal, S., Schmidt, I. K., Shi, H., Sternberg, M., Tian, H., Tschumi, E., Ukkola,

A., Vicca, S., Viovy, N., Wang, Y. P., Wang, Z., Williams, K., Wu, D., and Zhu, Q.: Rainfall manipulation experiments as simulated by terrestrial biosphere models: Where do we stand?, Global Change Biology, 26, 3336–3355, https://doi.org/10.1111/gcb.15024, https://onlinelibrary-wiley-com.ezp1.lib.umn.edu/doi/full/10.1111/gcb.15024https://onlinelibrary-wiley-com.ezp1.lib.umn.edu/doi/abs/10.1111/gcb.15024https://onlinelibrary-wiley-com.ezp1.lib.umn.edu/doi/10.1111/gcb.15024, 2020.

Powell, T. L., Galbraith, D. R., Christoffersen, B. O., Harper, A., Imbuzeiro, H. M., Rowland, L., Almeida, S., Brando, P. M., da Costa, A. C. L., Costa, M. H., Levine, N. M., Malhi, Y., Saleska, S. R., Sotta, E., Williams, M., Meir, P., and Moorcroft, P. R.: Confronting model predictions of carbon fluxes with measurements of Amazon forests subjected to experimental drought, New Phytologist, 200, 350–365, https://doi.org/10.1111/nph.12390, 2013.

Prentice, I. C., Liang, X., Medlyn, B. E., and Wang, Y.-P.: Reliable, robust and realistic: the three R's of next-generation land-surface modelling, Atmospheric Chemistry and Physics, 15, 5987–6005, https://doi.org/10.5194/acp-15-5987-2015, https://www.atmos-chem-phys.net/15/5987/2015/, 2015.

Razavi, S., Sheikholeslami, R., Gupta, H. V., and Haghnegahdar, A.: VARS-TOOL: A toolbox for comprehensive, efficient, and robust sensitivity and uncertainty analysis, Environmental Modelling and Software, 112, 95–107, https://doi.org/10.1016/j.envsoft.2018.10.005, 2019.

Restrepo-Coupe, N., Levine, N. M., Christoffersen, B. O., Albert, L. P., Wu, J., Costa, M. H., Galbraith, D., Imbuzeiro, H., Martins, G., da Araujo, A. C., Malhi, Y. S., Zeng, X., Moorcroft, P., and Saleska, S. R.: Do dynamic global vegetation models capture the seasonality of carbon fluxes in the Amazon basin? A data-model intercomparison, Global Change Biology, 23, 191–208, https://doi.org/10.1111/gcb.13442, http://doi.wiley.com/10.1111/gcb.13442, 2017.

Rogers, A., Medlyn, B. E., Dukes, J. S., Bonan, G., von Caemmerer, S., Dietze, M. C., Kattge, J., Leakey, A. D. B., Mercado, L. M., Niinemets, l., Prentice, I. C., Serbin, S. P., Sitch, S., Way, D. A., and Zaehle, S.: A roadmap for improving the representation of photosynthesis in Earth system models, New Phytologist, 213, 22–42, https://doi.org/10.1111/nph.14283, http://doi.wiley.com/10.1111/nph.14283, 2017.

Sabot, M. E. B., De Kauwe, M. G., Pitman, A. J., Medlyn, B. E., Verhoef, A., Ukkola, A. M., and Abramowitz, G.: Plant profit maximization improves predictions of European forest responses to drought, New Phytologist, N/A, 1–18, https://doi.org/10.1111/nph.16376, https://onlinelibrary.wiley.com/doi/abs/10.1111/nph.16376, 2020.

Schwarz, P. A., Law, B. E., Williams, M., Irvine, J., Kurpius, M., and Moore, D.: Climatic versus biotic constraints on carbon and water fluxes in seasonally drought-affected ponderosa pine ecosystems, Global Biogeochemical Cycles, 18, 1–17, https://doi.org/10.1029/2004GB002234, 2004.

Sitch, S., Huntingford, C., Gedney, N., Levy, P. E., Lomas, M., Piao, S. L., Betts, R., Ciais, P., Cox, P. M., Friedlingstein, P., Jones, C. D., Prentice, I. C., and Woodward, F. I.: Evaluation of the terrestrial carbon cycle, future plant geography and climate-carbon cycle feedbacks using five Dynamic Global Vegetation Models (DGVMs), Global Change Biology, 14, 2015–2039, https://doi.org/10.1111/j.1365-2486.2008.01626.x, http://doi.wiley.com/10.1111/j.1365-2486.2008.01626.x, 2008.

Sperry, J. S. and Love, D. M.: What plant hydraulics can tell us about responses to climate-change droughts, New Phytologist, 207, 14–27, https://doi.org/10.1111/nph.13354, http://doi.wiley.com/10.1111/nph.13354, 2015.

Sperry, J. S., Adler, F. R., Campbell, G. S., and Comstock, J. P.: Limitation of plant water use by rhizosphere and xylem conductance: Results from a model, Plant, Cell and Environment, 21, 347–359, https://doi.org/10.1046/j.1365-3040.1998.00287.x, 1998.

Trugman, A. T., Medvigy, D., Mankin, J. S., and Anderegg, W. R.: Soil Moisture Stress as a Major Driver of Carbon Cycle Uncertainty, Geophysical Research Letters, 45, 6495–6503, https://doi.org/10.1029/2018GL078131, 2018.

Ukkola, A. M., De Kauwe, M. G., Pitman, A. J., Best, M. J., Abramowitz, G., Haverd, V., Decker, M., and Haughton, N.: Land surface models systematically overestimate the intensity, duration and magnitude of seasonal-scale evaporative droughts, Environmental Research Letters, 11, 104 012, https://doi.org/10.1088/1748-9326/11/10/104012, https://iopscience.iop.org/article/10.1088/1748-9326/11/10/104012https://iopscience.iop.org/article/10.1088/1748-9326/11/10/104012/meta, 2016.

Ukkola, A. M., Haughton, N., De Kauwe, M. G., Abramowitz, G., and Pitman, A. J.: FluxnetLSM R package (v1.0): a community tool for processing FLUXNET data for use in land surface modelling, Geosci. Model Dev, 10, 3379–3390, https://doi.org/10.5194/gmd-10-3379-2017, https://doi.org/10.5194/gmd-10-3379-2017, 2017.

Verhoef, A. and Egea, G.: Modeling plant transpiration under limited soil water: Comparison of different plant and soil hydraulic parameterizations and preliminary implications for their use in land surface models, Agricultural and Forest Meteorology, 191, 22–32, https://doi.org/10.1016/J.AGRFORMET.2014.02.009, https://www.sciencedirect.com/science/article/pii/S0168192314000483, 2014.

Williams, M., Law, B. E., Anthoni, P. M., and Unsworth, M. H.: Use of a simulation model and ecosystem flux data to examine carbon-water interactions in ponderosa pine, Tree Physiology, 21, 287–298, https://doi.org/10.1093/treephys/21.5.287, 2001.

Wolf, A., Anderegg, W. R. L., and Pacala, S. W.: Optimal stomatal behavior with competition for water and risk of hydraulic impairment., Proceedings of the National Academy of Sciences of the United States of America, 113, E7222–E7230, https://doi.org/10.1073/pnas.1615144113, http://www.ncbi.nlm.nih.gov/pubmed/27799540, 2016.

Xu, X., Medvigy, D., Powers, J. S., Becknell, J. M., and Guan, K.: Diversity in plant hydraulic traits explains seasonal and inter-annual variations of vegetation dynamics in seasonally dry tropical forests, New Phytologist, 212, 80–95, https://doi.org/10.1111/nph.14009, http://doi.wiley.com/10.1111/nph.14009, 2016.

Yang, S. J. and de Jong, E.: Effect of Aerial Environment and Soil Water Potential on the Transpiration and Energy Status of Water in Wheat Plants 1, Agronomy Journal, 64, 574–578, https://doi.org/10.2134/agronj1972.00021962006400050006x, http://doi.wiley.com/10.2134/agronj1972.00021962006400050006x, 1972.

Zhang, Q., Manzoni, S., Katul, G., Porporato, A., and Yang, D.: The hysteretic evapotranspiration-Vapor pressure deficit relation, Journal of Geophysical Research: Biogeosciences, 119, 125–140, https://doi.org/10.1002/2013JG002484, http://doi.wiley.com/10.1002/2013JG002484, 2014.

Zhou, S., Duursma, R. A., Medlyn, B. E., Kelly, J. W., and Prentice, I. C.: How should we model plant responses to drought? An analysis of stomatal and non-stomatal responses to water stress, Agricultural and Forest Meteorology, 182-183, 204–214, https://doi.org/10.1016/J.AGRFORMET.2013.05.009, https://www.sciencedirect.com/science/article/pii/S0168192313001263, 2013.